2019 1ˢᵗ Season Stock Assessment

Falkland calamari

(*Doryteuthis gahi*)
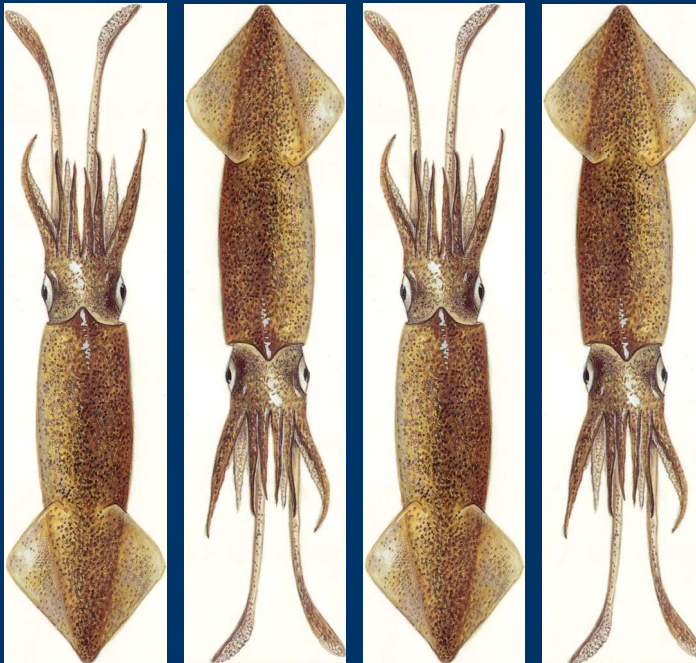
S1 - 2019 - LOL

Andreas Winter

Natural Resources - Fisheries
Falkland Islands Government
Stanley, Falkland Islands

November 2019

DESIRE THE RIGHT

Index

Summary

1) The 2019 first season *Doryteuthis gahi* fishery (C license) was open from February 24th, and closed by directed order on April 28th. Compensatory days for mechanical problems and bad weather resulted in 36 vessel-days taken after April 28th, with two vessels fishing as late as May 2nd.
2) Two fishing mortalities of Southern sea lions and five fishing mortalities of South American fur seals were recorded throughout the course of the season. The use of Seal Exclusion Devices was mandated north of 52° S starting on March 16th, and mandated south of 52° S starting on March 29th at 1400.
3) 55,586 tonnes of *D. gahi* catch were reported in the C-license fishery; the highest first season catch since 1995 and giving an average CPUE of 58.3 t vessel-day[-1]. During the season 37.8% of *D. gahi* catch and 38.1% of fishing effort were taken north of 52° S; 62.2% of *D. gahi* catch and 61.9% of fishing effort were taken south of 52° S.
4) In the south sub-area, four depletion periods / immigrations were inferred to have started on February 24th (start of the season), April 1st, April 5th, and April 14th. In the north sub-area, four depletion periods / immigrations were inferred to have started on March 9th (start of fishing), April 3rd, April 11th, and April 21st.
5) Approximately 139,959 tonnes of *D. gahi* (95% confidence interval: 98,376 to 318,368 t) were estimated to have immigrated into the Loligo Box during first season 2019, of which 84,441 t north of 52° S and 55,517 t south of 52° S.
6) The escapement biomass estimate for *D. gahi* remaining in the Loligo Box at the end of first season 2019 was:
   Maximum likelihood of 86,476 tonnes, with a 95% confidence interval of 69,575 to 187,644 tonnes.
    The risk of *D. gahi* escapement biomass at the end of the season being less than 10,000 tonnes was estimated at zero.

Introduction

The first season of the 2019 *Doryteuthis gahi* fishery (Patagonian longfin squid – colloquially *Loligo*) opened on February 24th. During the season 5 flex days were taken for mechanical repairs by various vessels, and one vessel delayed entry by 3 days due to bad weather in route. Thirty-seven flex days were taken for in-season bad weather, of which 16 on April 6th, 15 on April 7th, and 6 on April 18th (Figure 1). The season ended by directed closure on April 28th. The various schedule adjustments amounted to 36 vessel-days being taken after April 28th, with the last two vessels finishing on May 2nd.

As in previous seasons (Winter 2018a, b), all C-license vessels were required to embark an observer tasked (at minimum) to monitor the presence and incidental capture of pinnipeds. The occurrence of pinniped mortalities resulted in mandatory use of Seal Exclusion Devices (SEDs) north of 52°S starting on March 16th, and south of 52°S starting on March 29th (that is to say everywhere in the fishery from March 29th). Fishing was closed north of 52°S on April 26th, two days before the directed season end, because of small sizes of the squid (Figure 2).

Total reported *D. gahi* catch under first season C license was 20,986 north + 34,600 south = 55,586 tonnes (Table 1), the highest since 1995, and corresponding to an average CPUE of 55586 / 953 = 58.3 tonnes vessel-day[-1]. Average CPUE was the highest on record for either first or second season, and the increasing trend of the past few years (Table 1) suggests connection to the global proliferation of cephalopods (Doubleday et al. 2016).
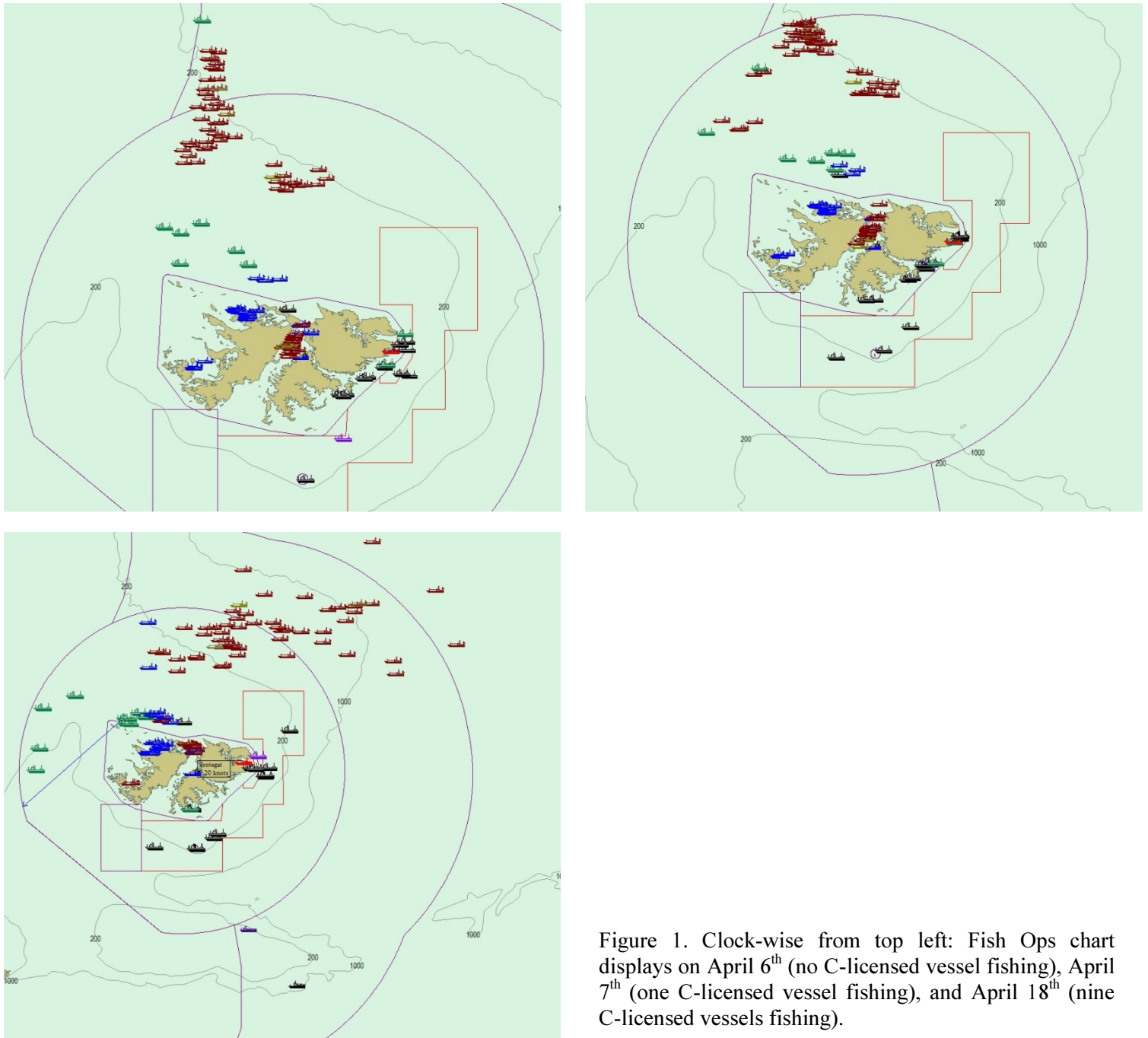
Figure 1. Clock-wise from top left: Fish Ops chart displays on April 6th (no C-licensed vessel fishing), April 7th (one C-licensed vessel fishing), and April 18th (nine C-licensed vessels fishing).

Assessment of the Falkland Islands *D. gahi* stock was conducted with depletion time-series models as in previous seasons (Agnew et al. 1998, Roa-Ureta and Arkhipkin 2007; Arkhipkin et al. 2008), and in other squid fisheries (Royer et al. 2002, Young et al. 2004, Chen et al. 2008, Morales-Bojórquez et al. 2008, Keller et al. 2015, Medellín-Ortiz et al. 2016). Because *D. gahi* has an annual life cycle (Patterson 1988, Arkhipkin 1993), stock cannot be derived from a standing biomass carried over from prior years (Rosenberg et al. 1990, Pierce and Guerra 1994). The depletion model instead calculates an estimate of population abundance over time by evaluating what levels of abundance and catchability must be extant to sustain the observed rate of catch. Depletion modelling of the *D. gahi* target fishery is used both in-season and for the post-season summary, with the objective of maintaining an escapement biomass of 10,000 tonnes *D. gahi* at the end of each season as a conservation threshold (Agnew et al. 2002, Barton 2002).

3
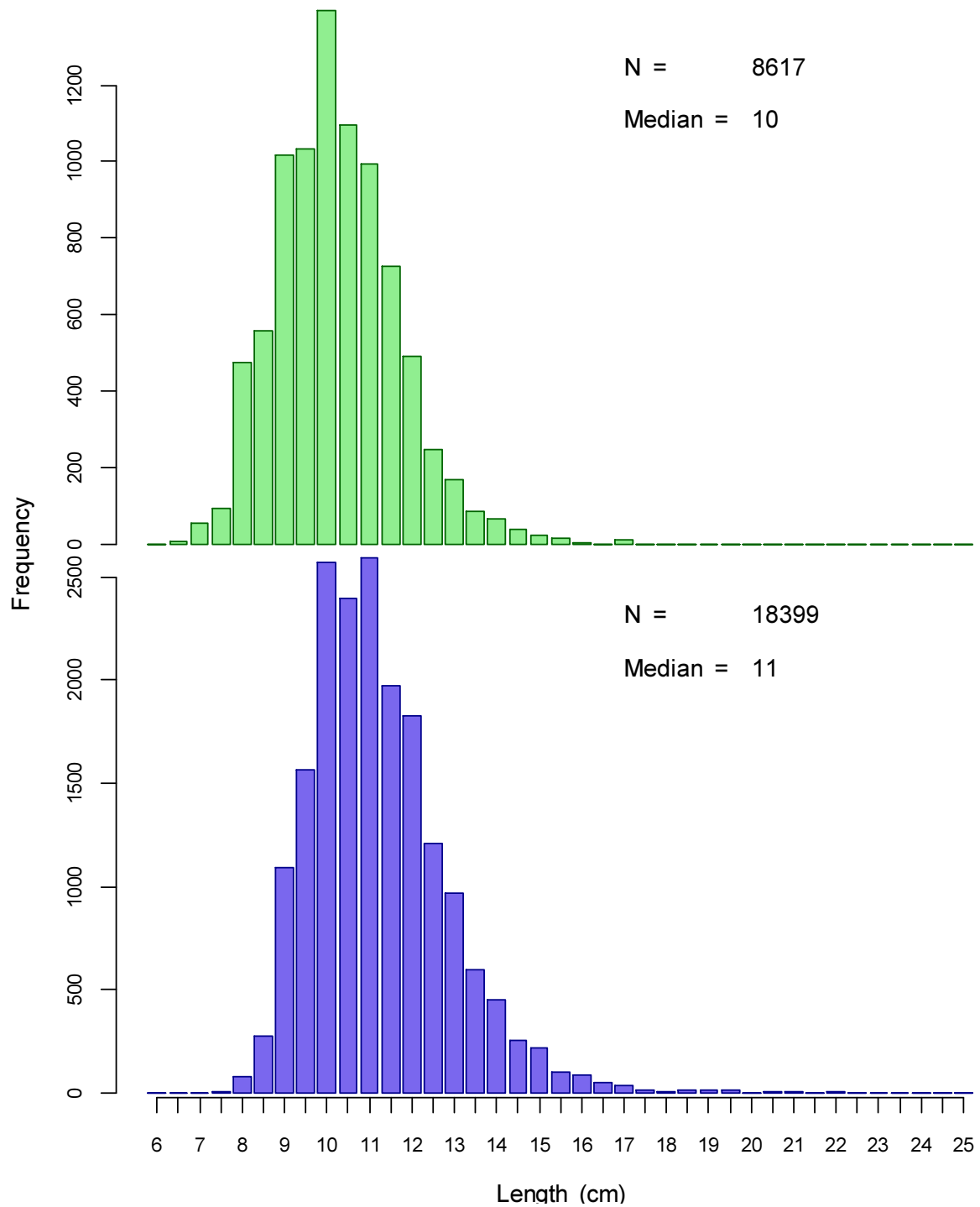
Figure 2. *D. gahi* observer length-frequency distributions from April 14th to April 22nd 2019, the date range over which the decision was made to close the north sub-area on April 26th. In the north (green – top) 25.7% of individuals had mantle lengths ≤ 9 cm. In the south (purple – bottom) 8.0% of individuals had mantle lengths ≤ 9 cm.

Methods

The depletion model formulated for the Falklands *D. gahi* stock is based on the equivalence:

$$C_{day} = q \times E_{day} \times N_{day} \times e^{-M/2} \tag{1}$$

where q is the catchability coefficient, M is the natural mortality rate (considered constant at 0.0133 day^{-1}; Roa-Ureta and Arkhipkin 2007), and C_{day}, E_{day}, N_{day} are catch (numbers of squid), fishing effort (numbers of vessels), and abundance (numbers of squid) per day. In its basic form (DeLury 1947) the depletion model assumes a closed population in a fixed area for the duration of the assessment. However, the assumption of a closed population is imperfectly met in the Falkland Islands fishery, where stock analyses have often shown that *D. gahi* groups arrive in successive waves after the start of the season (Roa-Ureta 2012; Winter and Arkhipkin 2015). Arrivals of successive groups are inferred from discontinuities in the catch data. Fishing on a single, closed cohort would be expected to yield gradually decreasing CPUE, but gradually increasing average individual sizes, as the squid grow. When instead these data change suddenly, or in contrast to expectation, the immigration of a new group to the population is indicated (Winter and Arkhipkin 2015).

Table 1. *D. gahi* season comparisons since 2004, when catch management was assumed by the FIFD. Days: total number of calendar days open to licensed *D. gahi* fishing including (since 1st season 2013) optional extension days; V-Days: aggregate number of licensed *D. gahi* fishing days reported by all vessels for the season. Entries in italics are seasons closed by emergency order.

	Season 1			Season 2		
	Catch (t)	Days	V-Days	Catch (t)	Days	V-Days
2004	7,152	46	625	17,559	78	1271
2005	24,605	45	576	29,659	78	1210
2006	19,056	50	704	*23,238*	*53*	*883*
2007	17,229	50	680	*24,171*	*63*	*1063*
2008	24,752	51	780	26,996	78	1189
2009	12,764	50	773	*17,836*	*59*	*923*
2010	28,754	50	765	36,993	78	1169
2011	15,271	50	771	*18,725*	*70*	*1099*
2012	34,767	51	770	35,026	78	1095
2013	19,908	53	782	19,614	78	1195
2014	28,119	59	872	19,630	71	1099
2015	*19,383**	*57**	*871**	*10,190*	*42*	*665*
2016	22,616	68	1020	23,089	68	1004
2017	39,433	68	999†	24,101	69	1002‡
2018	43,085	69	975	35,828	68	977
2019	55,586	68	953			

* Does not include C-license catch or effort after the C-license target for that season was switched from *D. gahi* to *Illex*.
† Includes two vessel-days of experimental fishing for juvenile toothfish.
‡ Includes one vessel-day of experimental fishing for juvenile toothfish.

In the event of a new group arrival, the depletion calculation must be modified to account for this influx. This is done using a simultaneous algorithm that adds new arrivals on top of the stock previously present, and posits a common catchability coefficient for the entire depletion time-series. If two depletions are included in the same model (i.e., the stock present from the start plus a new group arrival), then:

$$C_{day} = q \times E_{day} \times (N1_{day} + (N2_{day} \times i2\big|_0^1)) \times e^{-M/2} \tag{2}$$

where i2 is a dummy variable taking the values 0 or 1 if 'day' is before or after the start day of the second depletion. For more than two depletions, $N3_{day}$, i3, $N4_{day}$, i4, etc., would be included following the same pattern.

Because SEDs were mandated in this season, the SED modification of the depletion model (Winter 2017b) was implemented again for the stock assessment:

$$C_{day} = q_{SED} \times E_{SED-day} \times (N1_{day} + (N2_{day} \times i2|_0^1)) \times e^{-M/2} \tag{3}$$
$$+ q_{NSED} \times E_{NSED-day} \times (N1_{day} + (N2_{day} \times i2|_0^1)) \times e^{-M/2}$$

whereby the depletion catch Equation **2** is formulated as the composite of fishing effort in parallel with and without SEDs (subscripts SED and NSED). As before, the computational difference between q_{SED} and q_{NSED} includes not only the technical efficacy of either gear but all fishing aspects that correlate with the gear; e.g., that vessels fishing under SED 'conditions' might stop a trawl when pinnipeds are sighted, or switch locations more frequently or distantly.

The season depletion likelihood function was calculated as the difference between actual catch numbers reported and catch numbers predicted from the model (Equation **3**), statistically corrected by a factor relating to the number of days of the depletion period (Roa-Ureta 2012):

$$((n\text{Days} - 2)/2) \times \log\left(\sum_{days}\left(\log(\text{predicted}\,C_{day}) - \log(\text{actual}\,C_{day})\right)^2\right) \tag{4}$$

The stock assessment was set in a Bayesian framework (Punt and Hilborn 1997), whereby results of the season depletion model are conditioned by prior information on the stock; in this case the information from the pre-season survey.

The likelihood function of prior information was calculated as the normal distribution of the difference between catchability (q) derived from the survey abundance estimate, and catchability derived from the season depletion model. Applying this difference requires both the survey and the season to be fishing the same stock with the same gear. Catchability, rather than abundance N, is used for calculating prior likelihood because catchability informs the entire season time series; whereas N from the survey only informs the first in-season depletion period – subsequent immigrations and depletions are independent of the abundance that was present during the survey. In this season, only NSED fishing was conducted in the pre-season survey (Winter et al. 2019), and therefore only q_{NSED} could be linked to a prior. Thus, the prior likelihood function was:

$$\frac{1}{\sqrt{2\pi \cdot SD_{q\,prior\,NSED}^2}} \times \exp\left(-\frac{\left(q_{model\,NSED} - q_{prior\,NSED}\right)^2}{2 \cdot SD_{q\,prior\,NSED}^2}\right) \tag{5}$$

where the standard deviation of catchability prior ($SD_{q\,prior\,NSED}$) was calculated from the Euclidean sum of the survey prior estimate uncertainty, the variability in catches on the season start date, and the uncertainty in the natural mortality M estimate over the number of days mortality discounting (Appendix: Equations **A5-S**, **A5-N**).

Bayesian optimization of the depletion was calculated by jointly minimizing Equations **4** and **5**, using the Nelder-Mead algorithm in R programming package 'optimx' (Nash and Varadhan 2011). Relative weights in the joint optimization were assigned to

Equations **4** and **5** as the converse of their coefficients of variation (CV), i.e., the CV of the prior became the weight of the depletion model and the CV of the depletion model became the weight of the prior. Calculations of the CVs are described in Equations **A8-S** and **A8-N**. Because a complex model with multiple depletions may converge on a local minimum rather than global minimum, the optimization was stabilized by running a feed-back loop that set the q and N parameter outputs of the Bayesian joint optimization back into the in-season-only minimization (Equation **4**), re-calculated this minimization and the CV resulting from it, then re-calculated the Bayesian joint optimization, and continued this process until both the in-season minimization and the joint optimization remained unchanged.

With actual C_{day}, $E_{NSED\text{-}day}$, $E_{SED\text{-}day}$, and M being fixed parameters, the optimization of Equation **3** using **4** and **5** produces estimates of q_{NSED}, q_{SED}, and N1, N2, …, etc. Numbers of squid on the final day (or any other day) of a time series are then calculated as the numbers N of the depletion start days discounted for natural mortality during the intervening period, and subtracting cumulative catch also discounted for natural mortality (CNMD). Taking for example a two-depletion period:

$$
N_{final\ day} = \begin{aligned} &N1_{start\ day\ 1} \times e^{-M\,(final\ day\ -\ start\ day\ 1)} \\ +\ &N2_{start\ day\ 2} \times e^{-M\,(final\ day\ -\ start\ day\ 2)} \\ -\ &CNMD_{final\ day} \end{aligned} \tag{6}
$$

where

$$
CNMD_{day\ 1} = 0
$$

$$
CNMD_{day\ x} = CNMD_{day\ x-1} \times e^{-M} + C_{day\ x-1} \times e^{-M/2} \tag{7}
$$

$N_{final\ day}$ is then multiplied by the average individual weight of squid on the final day to give biomass. Daily average individual weight is obtained from length / weight conversion of mantle lengths measured in-season by observers, and also derived from in-season commercial data as the proportion of product weight that vessels reported per market size category. Observer mantle lengths are scientifically accurate, but restricted to 1-2 vessels at any one time that may or may not be representative of the entire fleet, and not available every day. Commercially proportioned mantle lengths are relatively less accurate, but cover the entire fishing fleet every day. Therefore, both sources of data are used (see Appendix – *Doryteuthis gahi* individual weights).

Distributions of the likelihood estimates from joint optimization (i.e., measures of their statistical uncertainty) were computed using a Markov Chain Monte Carlo (MCMC) (Gamerman and Lopes 2006), a method that is commonly employed for fisheries assessments (Magnusson et al. 2013). MCMC is an iterative process which generates random stepwise changes to the proposed outcome of a model (in this case, the q and N of *D. gahi* squid) and at each step, accepts or nullifies the change with a probability equivalent to how well the change fits the model parameters compared to the previous step. The resulting sequence of accepted or nullified changes (i.e., the 'chain') approximates the likelihood distribution of the model outcome. The MCMC of the depletion models were run for 200,000 iterations; the first 1000 iterations were discarded as burn-in sections (initial phases over which the algorithm stabilizes); and the chains were thinned by a factor equivalent to the maximum of either 5 or the inverse of the acceptance rate (e.g., if the acceptance rate was 12.5%, then every 8th (0.125^{-1}) iteration was retained) to reduce serial correlation. For each model three chains were run; one chain initiated with the parameter values obtained from the joint optimization of Equations **4** and **5**, one chain initiated with these parameters ×2, and one chain initiated with these parameters ×¼. Convergence of the three chains was accepted if the variance among

chains was less than 10% higher than the variance within chains (Brooks and Gelman 1998). When convergence was satisfied the three chains were combined as one final set. Equations **6**, **7**, and the multiplication by average individual weight were applied to the CNMD and each iteration of N values in the final set, and the biomass outcomes from these calculations represent the distribution of the estimate. The peaks of the MCMC histograms were compared to the empirical optimizations of the N values.

Commercial catch, 24/02 - 02/05 2019
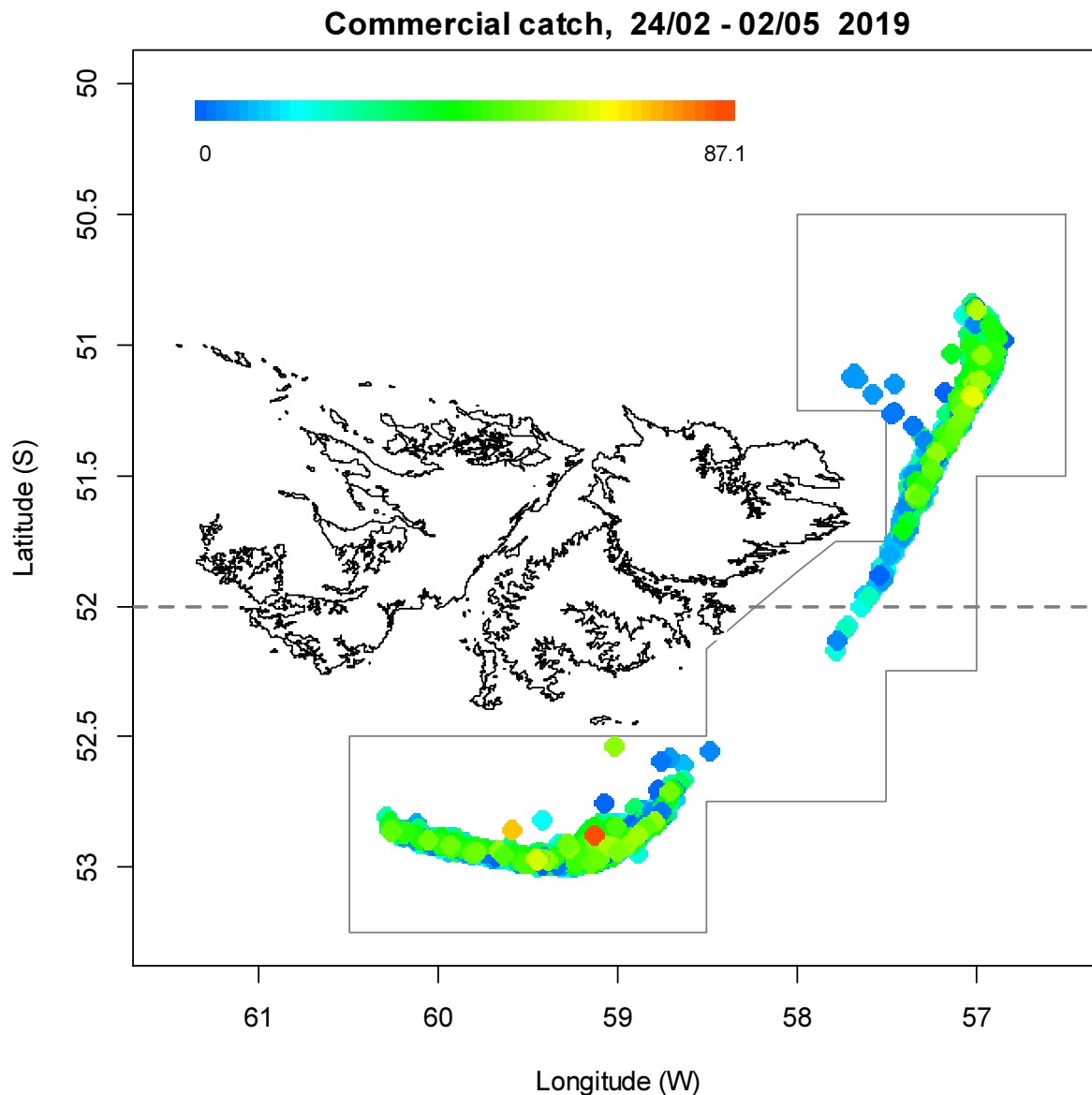
Figure 3. Spatial distribution of *D. gahi* 1st-season trawls, colour-scaled to catch weight (max. = 87.1 tonnes). 2685 trawl catches were taken during the season. The 'Loligo Box' fishing zone and the 52 ºS parallel delineating the boundary between north and south assessment sub-areas, are shown in grey.

Depletion models and likelihood distributions were calculated separately for north and south sub-areas of the Loligo Box fishing zone, as *D. gahi* sub-stocks emigrate from different spawning grounds and remain to an extent segregated (Arkhipkin and Middleton 2002). Total escapement biomass is then defined as the aggregate biomass of *D. gahi* on the last day of the

season for north and south sub-areas combined. North and south biomasses are not assumed to be uncorrelated however (Shaw et al. 2004), and therefore north and south likelihood distributions were added semi-randomly in proportion to the strength of their day-to-day correlation (see Winter 2014, for the semi-randomization algorithm).

As previous seasons had shown relatively modest differences between catchabilities q_{SED} and q_{NSED} (Winter 2018a, b), a comparison was also calculated between the *D. gahi* biomass estimated with separately parametrized q_{SED} and q_{NSED}, and *D. gahi* biomass estimated with a single undifferentiated q; i.e., the difference between Equations **2** and **3**.
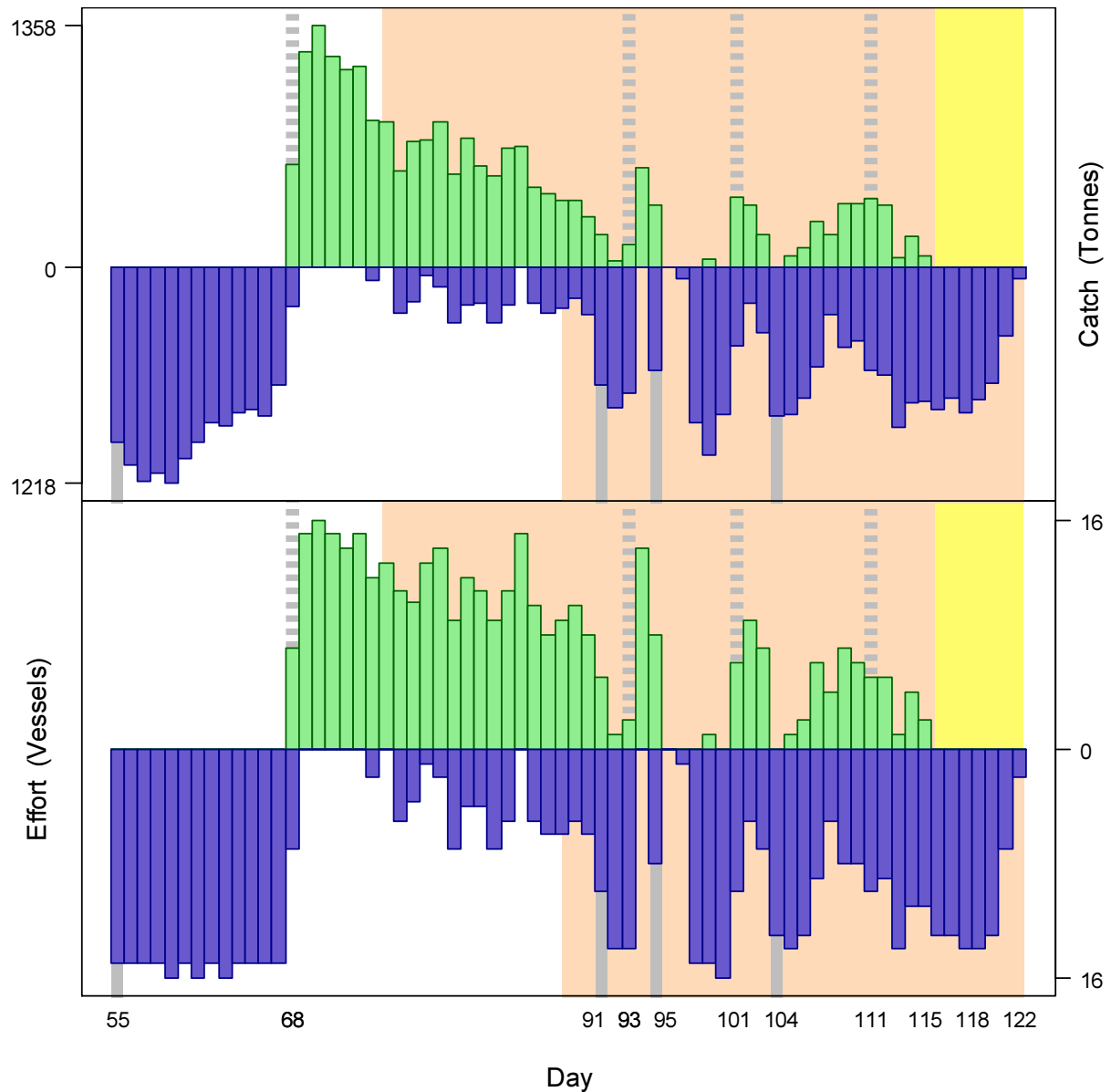

Figure 4. Daily total *D. gahi* catch and effort distribution by assessment sub-area north (green) and south (purple) of the 52° S parallel during 1st season 2019. The season was open from February 24th (chronological day 55) to April 28th (chronological day 118), plus flex days until May 2nd (day 122). Orange under-shading delineates the mandatory use of SEDs north and south. Yellow under-shading delineates the early closure of the north sub-area. As many as 16 vessels fished per day north; as many as 16 vessels fished per day south. As much as 1358 tonnes *D. gahi* was caught per day north; as much as 1218 tonnes *D. gahi* was caught per day south.

Stock assessment
Data

The north sub-area was fished on 43 of the 68 season-days, for 37.8% of the total catch (20986.0 t *D. gahi*) and 38.1% of the effort (363.3 vessel-days) (Figure 3). 79.5% of north catch was taken in the first 24 days (March 9th to April 1st; Figure 4). The south sub-area was fished on 59 of the 68 season-days, for 62.2% of total catch (34599.6 t *D. gahi*) and 61.9% of effort (589.7 vessel-days). 37.3% of south catch was taken in the first 14 days (February 24th to March 9th; Figure 4).

953 vessel-days were fished during the season (Table 1), with a median of 15 vessels per day (mean 14.33) except for flex and weather extensions. Vessels reported daily catch totals to the FIFD and electronic logbook data that included trawl times, positions, depths, and product weight by market size categories. Three FIG fishery observers were deployed in the fishing season for a total of 49 sampling days[a] (Hall 2019, Roberts 2019, Tutjavi 2019). Throughout the 68 days of the season, 19 days had no FIG fishery observer covering (including 1 of the 4 season-end extension days), 44 days had 1 FIG fishery observer covering, 4 days had two FIG fishery observers covering, and 1 day had three FIG observers covering. Except for seabird days FIG fishery observers were tasked with sampling 200 *D. gahi* at two stations; reporting their maturity stages, sex, and lengths to 0.5 cm. Contract marine mammal monitors were tasked with measuring 200 unsexed lengths of *D. gahi* per day. The length-weight relationship for converting observer and commercially proportioned lengths was combined from 1st pre-season and season length-weight data of both 2018 and 2019, as 2019 data became available progressively with on-going observer coverage. The final parameterization of the length-weight relationship included 3183 measures from 2018 and 1494 measures from 2019, giving:

$$\text{weight (kg)} \quad = \quad 0.14795 \times \text{length (cm)}^{2.28394} / 1000 \qquad \textbf{(8)}$$

with a coefficient of determination $R^2 = 94.4\%$.

Group arrivals / depletion criteria

Start days of depletions - following arrivals of new *D. gahi* groups - were judged primarily by daily changes in CPUE, with additional information from sex proportions, maturity, and average individual squid sizes. CPUE was calculated as metric tonnes of *D. gahi* caught per vessel per day. Days were used rather than trawl hours as the basic unit of effort. Commercial vessels do not trawl standardized duration hours, but rather durations that best suit their daily processing requirements. An effort index of days is therefore more consistent.

Four days in the south and four days in the north were identified that represented the onset of separate immigrations / depletions throughout the season.

- The first depletion south was set on day 55 (February 24th), the first day of the season with all vessels fishing south. CPUE was high and increased for the next 3 days (Figure 5). Average individual weight (observer measured), female proportion, and maturity all showed increasing trends for approximately the next week (Figures 6B, C and D).
- The second depletion south was identified on day 91 (April 1st), with a sharp increase in CPUE (Figure 5) and an increase in average individual weight (commercial) (Figure 6A).

---

[a] Not counting seabird days (every fourth day).

- The third depletion south was identified on day 95 (April 5th) with the highest CPUE in 36 days (and following a day when no fishing effort was taken in the south) (Figure 5). Average individual weight (observer measured) had decreased to a local minimum, and the female proportion increased to the highest in 32 days (Figures 6B and C).
- The fourth depletion south was identified on day 104 (April 14th) with a moderate CPUE peak (Figure 5), and following pronounced decreases in commercial and observer measured average individual weight (Figures 6A and B).
- The first depletion north was set on day 68 (March 9th), the first day of fishing in the north sub-area, by seven vessels. CPUE was second-highest for the season (Figure 5). Average weight, proportion female and maturity all reached maxima within the following three days (Figures 6A, B, C and D).
- The second depletion north was identified on day 93 (April 3rd) with a peak in CPUE after a declining trend since the start of fishing in the north (albeit a peak that was fished by only two vessels) (Figure 5). Average individual weight (commercial) was at its minimum for the season the day before (Figure 6A).
- The third depletion north was identified on day 101 (April 11th) with the highest CPUE in 24 days (whereby only one vessel-day of fishing had been taken in the preceding 5 days) (Figure 5). Average individual weight (commercial) was the lowest since the previous depletion north (Figure 6A).
- The fourth depletion north was identified on day 111 (April 21st) with the highest CPUE since shortly after the first depletion (Figure 5). Average individual weight (observer measured) and male maturity were the lowest of the season (Figures 6B and D).
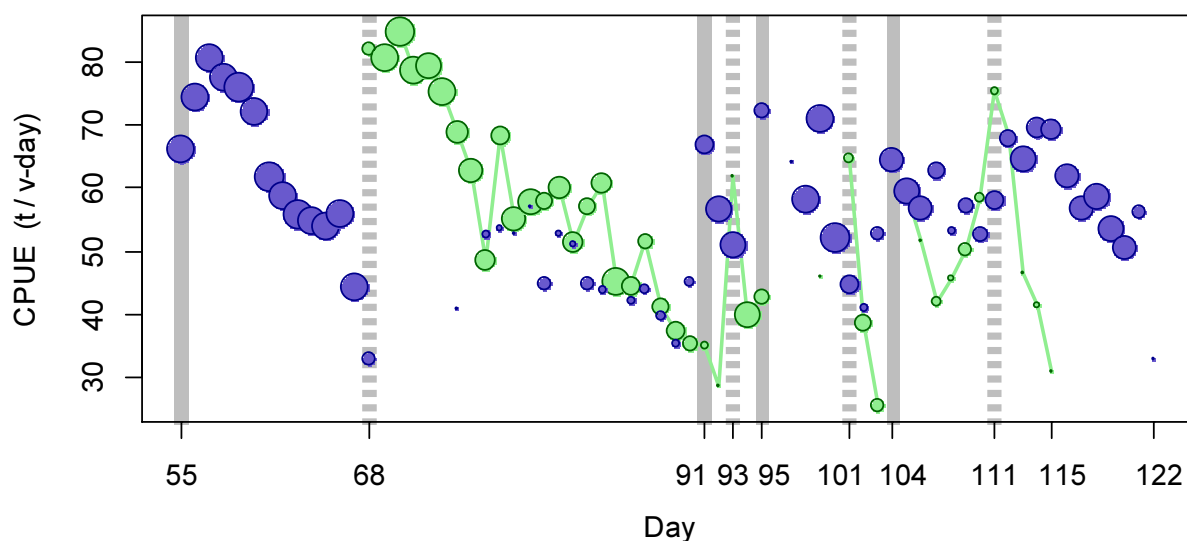

Figure 5. CPUE in metric tonnes per vessel per day, by assessment sub-area north (green) and south (purple) of 52° S latitude. Circle sizes are proportioned to numbers of vessels fishing. Data from consecutive days are joined by line segments. Broken grey bars indicate the starts of in-season depletions north. Solid grey bars indicate the starts of in-season depletions south.

Figure 6 [next page]. A: Average individual *D. gahi* weights (kg) per day from commercial size categories. B: Average individual *D. gahi* weights (kg) by sex per day from observer sampling. C: Proportions of female *D. gahi* per day from observer sampling. D: Average maturity value by sex per day from observer sampling. Males: triangles, females: squares, unsexed: circles. North sub-area: green, south sub-area: purple. Data from consecutive days are joined by line segments. Broken grey bars: the starts of in-season depletions north. Solid grey bars: the starts of in-season depletions south.
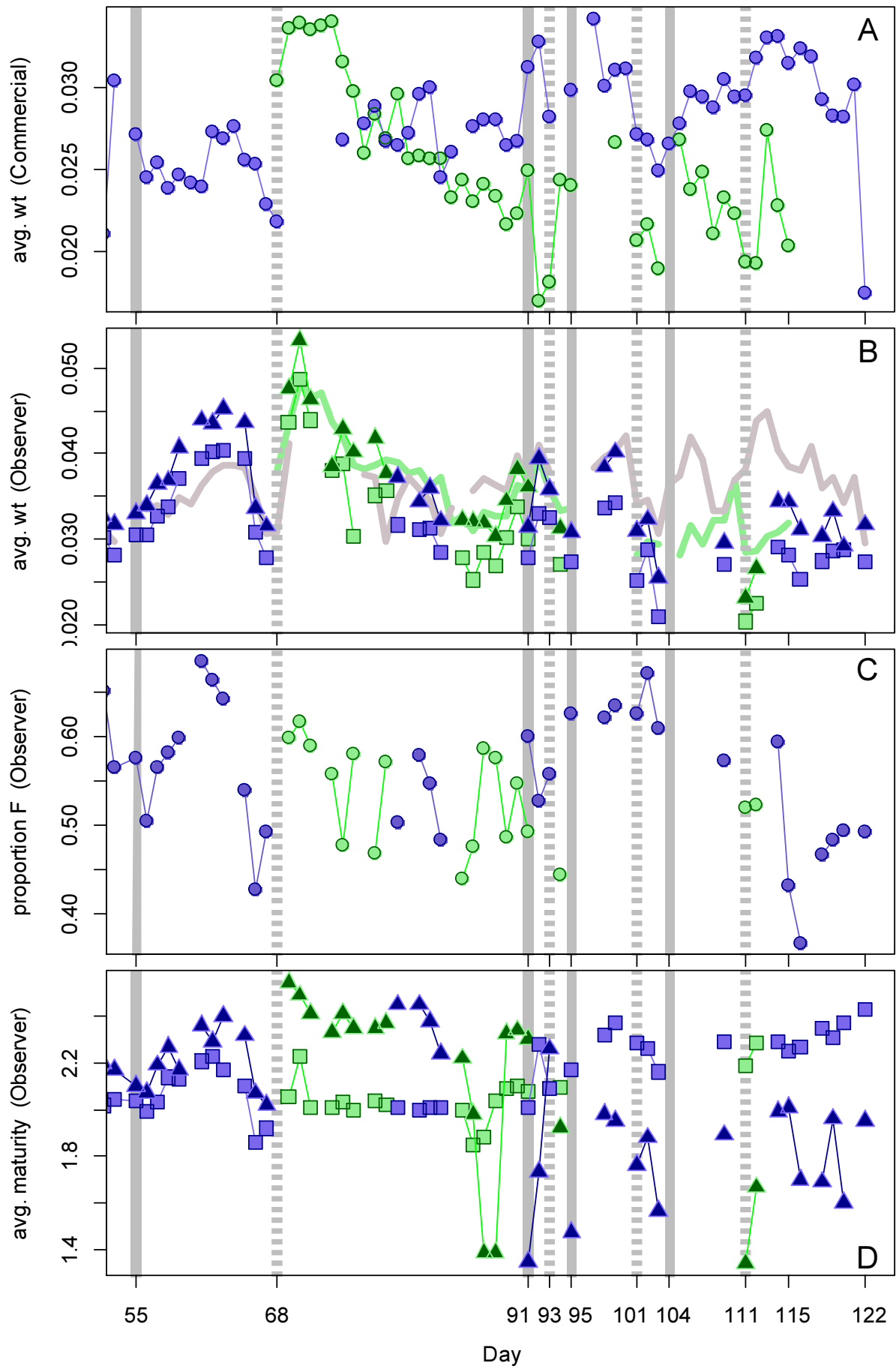
Depletion analyses

South

In the south sub-area, Bayesian optimization was weighted more to in-season depletion at 0.507 (**A5-S**) vs. the prior at 0.146 (**A8-S**). Bayesian optimization on catchability q without SEDs resulted in a maximum likelihood posterior ($_{Bayesian}$ q $_{S NSED}$ = 1.182 × 10^{-3}; Figure 7, left, and Equation **A9-S**) that was well centred between the pre-season prior ($_{prior}$ q $_S$ = 1.640 × 10^{-3}; Figure 7, left, and Equation **A4-S**) and the in-season depletion ($_{depletion}$ q $_{S NSED}$ = 0.702 × 10^{-3}; Figure 7, left, and **A6-S**).
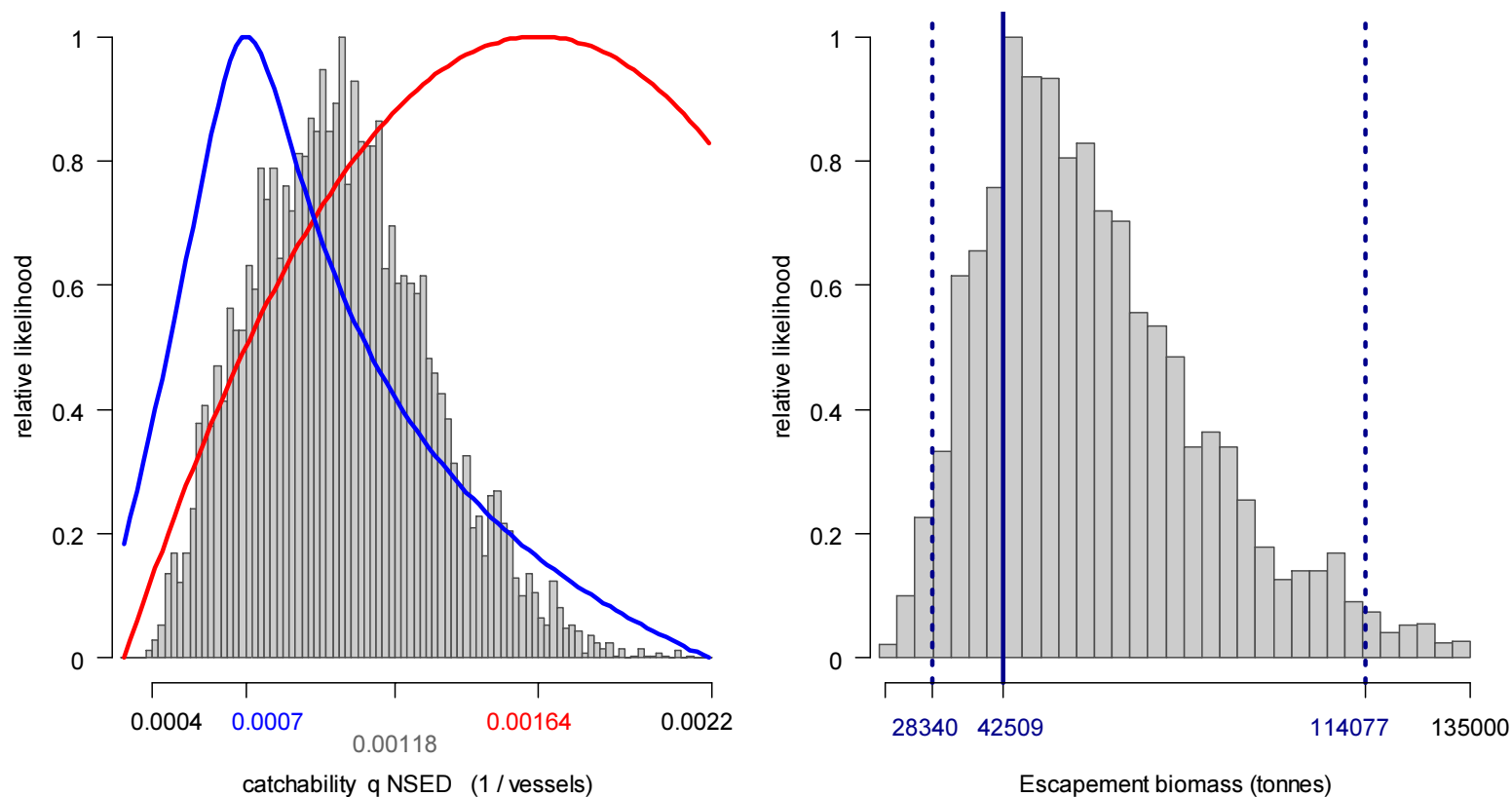

Figure 7. South sub-area. Left: Likelihood distributions for *D. gahi* NSED catchability. Red line: prior model (pre-season survey data), blue line: in-season depletion model, grey bars: combined Bayesian model posterior. Right: Likelihood distribution (grey bars) of escapement biomass, from Bayesian posterior and average individual squid weight at the end of the season. Blue lines: maximum likelihood and 95% confidence interval. Note correspondence to Figure 8.

The MCMC distribution of the Bayesian posterior multiplied by the GAM fit of average individual squid weight (Figure A1-south) gave the likelihood distribution of *D. gahi* biomass on day 122 (May 2nd) shown in Figure 7-right, with maximum likelihood and 95% confidence interval of:

$$B_{S day 122} \quad = \quad 42{,}509 \text{ t} \sim 95\% \text{ CI } [28{,}340 - 114{,}077] \text{ t} \tag{9}$$

13

On the first day of the season estimated *D. gahi* biomass south was 67,724 t ~ 95% CI [52,990 – 135,537] t (Figure 8); significantly higher than the pre-season estimate of 44,998 t (Winter et al. 2019). At its highest point (the last immigration of the season: day 104 – April 14th), estimated *D. gahi* biomass south was 71,044 t ~ 95% CI [51,589 – 169,309] t. Variability remained high throughout the time period, and it is not statistically conclusive that any change in average biomass occurred during the season by the rule that a straight line could be drawn through the plot (Figure 8) without intersecting the 95% confidence intervals (Swartzman et al. 1992).
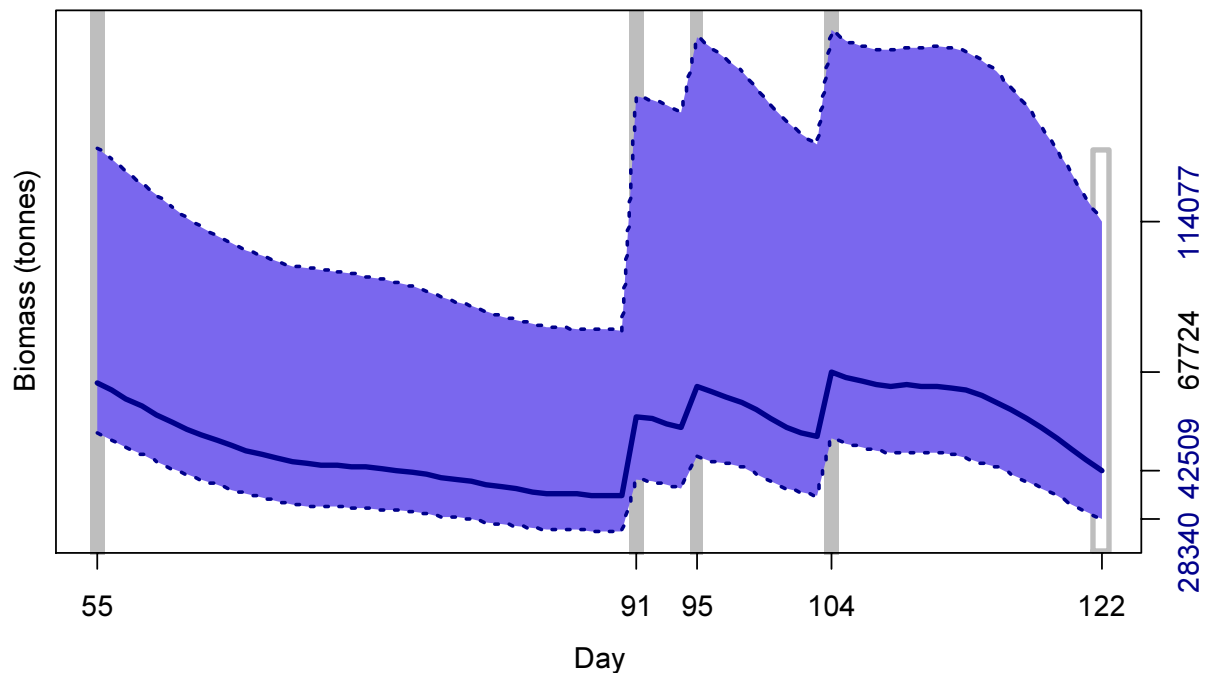

Figure 8. South sub-area. *D. gahi* biomass time series estimated from Bayesian posterior of the depletion model ± 95% confidence intervals. Grey bars indicate the start of in-season depletions south; days 55, 91, 95, 104, and 122. Note that the biomass 'footprint' on day 122 (May 2nd) corresponds to the right-side plot of Figure 7.

Posterior catchability with SEDs was $_{Bayesian}q_{S\ SED} = 0.960 \times 10^{-3}$ (Equation **A9-S**), thus lower than $_{Bayesian}q_{S\ NSED}$. Depletion modelling with single catchability for all trawls obtained $_{Bayesian}q_S = 1.149 \times 10^{-3}$, higher than both $_{Bayesian}q_{S\ NSED}$ and $_{Bayesian}q_{S\ SED}$. The biomass time series estimated with single catchability depletion modelling started to diverge from the $_{NSED}/_{SED}$ biomass time series starting from the second immigration (day 91, Figure A3-S), which occurred shortly after the switch to SEDs was mandated. Thereafter, the ratio by which biomass estimated from single catchability was lower than biomass estimated with $_{NSED}/_{SED}$ roughly equated to the ratio between $_{Bayesian}q_{S\ SED}$ and $_{Bayesian}q_S$: 0.960/1.149 = 0.835; $B_{S\ single\ q\ day\ 122}/B_{S\ day\ 122} = 34758/42509 = 0.818$. Notably, biomass time series calculated either way did not differ statistically, being entirely bounded by both sets of 95% confidence intervals (Figure A3-S).

North

In the north sub-area, Bayesian optimization was weighted at 1.010 for in-season depletion (**A5-N**) vs. 0.202 for the prior (**A8-N**). Bayesian optimization on catchability (q) without

SEDs resulted in a maximum likelihood posterior of $_{Bayesian}q_{N\,NSED} = 0.925 \times 10^{-3}$ (Figure 9, left, and Equation **A9-N**). With the 'borrowed' prior – see Appendix ($_{prior}q_N = _{prior}q_S = 1.640 \times 10^{-3}$; Figure 9, left, and Equation **A4-N**) being proportionally low-weighted due to its high uncertainty load, the posterior was nevertheless roughly halfway between the in-season estimate and the prior, as in-season $q_{N\,NSED}$ ($_{depletion}q_{N\,NSED} = 0.320 \times 10^{-3}$; Figure 9, left, and **A6-N**) had only a relatively short period to influence the model before SEDs were mandated (Figure 4). The relatively poor model fit resulted in a right-skewed distribution mode (Figure 9 left).
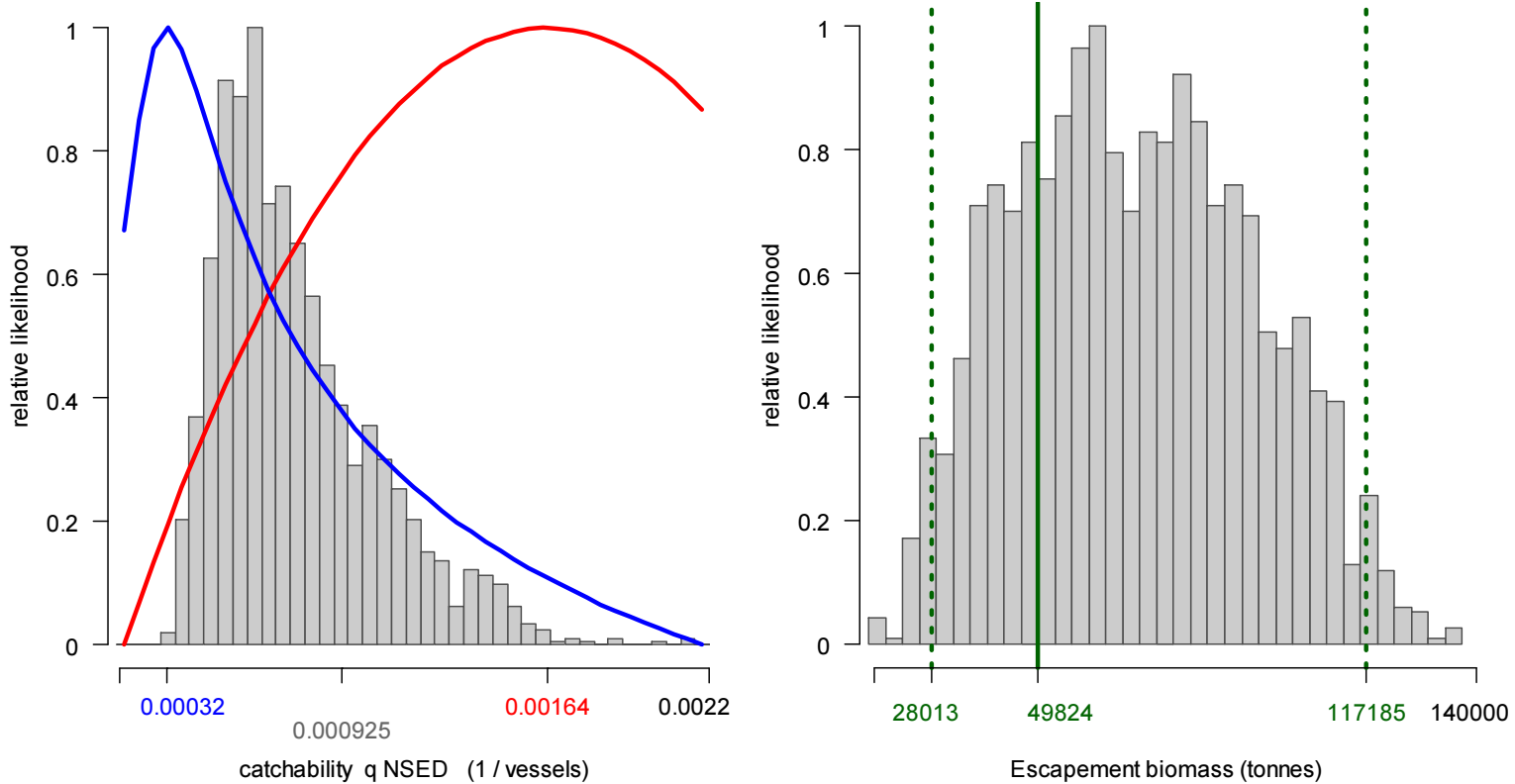

Figure 9. North sub-area. Left: Likelihood distributions for *D. gahi* NSED catchability. Red line: prior model (pre-season survey data), blue line: in-season depletion model, grey bars: combined Bayesian model posterior. Right: Likelihood distribution (grey bars) of escapement biomass, from Bayesian posterior and average individual squid weight at the end of the season. Green lines: maximum likelihood and 95% confidence interval. Note the correspondence to Figure 10.

The MCMC distribution of the Bayesian posterior multiplied by the generalized additive model (GAM) fit of average individual squid weight (Figure A1-north) gave the likelihood distribution of *D. gahi* biomass on day 115 (April 25th; the day fishing ended in the north) shown in Figure 9-right, with maximum likelihood and 95% confidence interval of:

$$B_{N\,day\,115} \quad = \quad 49,823\,t \sim 95\%\,CI\,[28,013 - 117,185]\,t \quad \textbf{(10)}$$

With no further catch but continuing natural mortality, the maximum likelihood biomass by the overall last day of the season (day 122, May 2nd) progressed to:

$$B_{N\,day\,122} \quad = \quad 44,545\,t \sim 95\%\,CI\,[25,021 - 104,845]\,t \quad \textbf{(11)}$$

15

At its highest point (the start of fishing: day 68 – March 9th), model-estimated *D. gahi* biomass north was 95,895 t ~ 95% CI [61,776 – 209,977] t (Figure 10). As in the south, variation of the average biomass time series trend was not statistically significant.
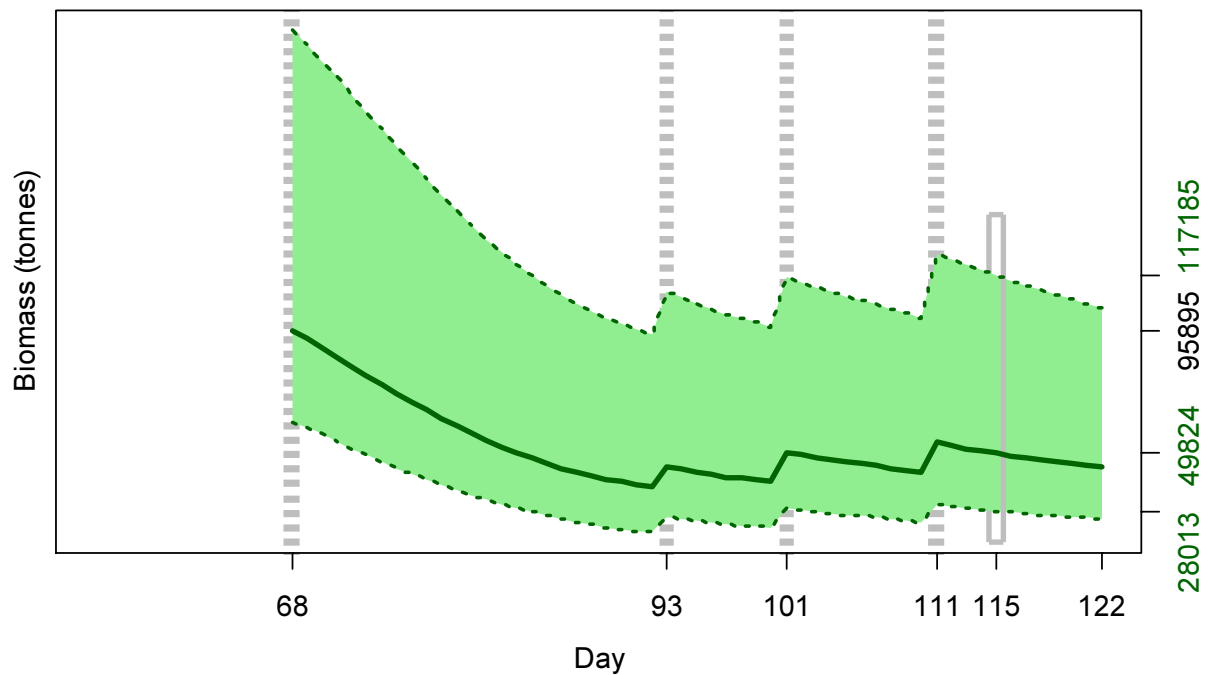

Figure 10. North sub-area. *D. gahi* biomass time series estimated from Bayesian posterior of the depletion model ± 95% confidence intervals. Broken grey bars indicate the start of in-season depletions north; days 68, 93, 101and 111. Note that the biomass 'footprint' on day 115 (April 25th) corresponds to the right-side plot of Figure 9.

Posterior catchability with SEDs was slightly higher at $_{Bayesian}$ q $_{N\ SED}$ = 0.990 × 10^{-3} (Equation **A9-N**). Depletion modelling with single catchability for all trawls obtained $_{Bayesian}$ q $_N$ = 0.756 × 10^{-3}, lower than both $_{Bayesian}$ q $_{N\ NSED}$ and $_{Bayesian}$ q $_{N\ SED}$. As the switch to SEDs occurred soon in the north after the start of fishing, the entire biomass time series diverged consistently when estimated with single catchability, although, as in the south, the difference was never statistically significant (Figure A3-N). The ratio by which biomass estimated from single catchability was higher than biomass estimated with $_{NSED}$ / $_{SED}$ again roughly equated to the ratio between $_{Bayesian}$ q $_{N\ SED}$ and $_{Bayesian}$ q $_N$: 0.990/0.756 = 1.309; B $_{N\ single\ q\ day\ 122}$ / B $_{N\ day\ 122}$ = 58476/44545 = 1.313.

Escapement biomass

Total escapement biomass was defined as the aggregate biomass of *D. gahi* at the end of day 122 (May 2nd) for south and north sub-areas combined (Equations **9** and **11**). Depletion models are calculated on the inference that all fishing and natural mortality are gathered at mid-day, thus a half day of mortality ($e^{-M/2}$) was added to correspond to the closure of the fishery at 23:59 (mid-night) on May 2nd for the final remaining vessels: Equation **12**.

$$B_{Total\ day\ 122} = (B_{S\ day\ 122} + B_{N\ day\ 122}) \times e^{-M/2}$$

$$= \quad 87{,}054 \, t \; \times \; 0.99336$$

$$= \quad 86{,}476 \, t \; \sim \; 95\% \; CI \; [69{,}575 - 187{,}6441] \, t \qquad \textbf{(12)}$$

South and north biomass season time series were overall negatively correlated with each other (R = –0.347), and on their final days both south and north had maximum likelihood biomass estimates lower than the modes of their likelihood distributions (Figures 7-right and 9-right). Semi-randomized addition of these distributions with negative correlation gave the aggregate likelihood of total escapement biomass shown in Figure 11. The aggregate distribution was symmetrical but maximum likelihood (86,476 tonnes) placed substantively lower than the distribution mode, evidence that in a season with little realized depletion the model fit is not strong.

The estimated escapement biomass of 86,476 t was the highest since at least 2005. The risk of the fishery in the current season, defined as the proportion of the total escapement biomass distribution below the conservation limit of 10,000 tonnes (Agnew et al., 2002; Barton, 2002), was calculated as zero.
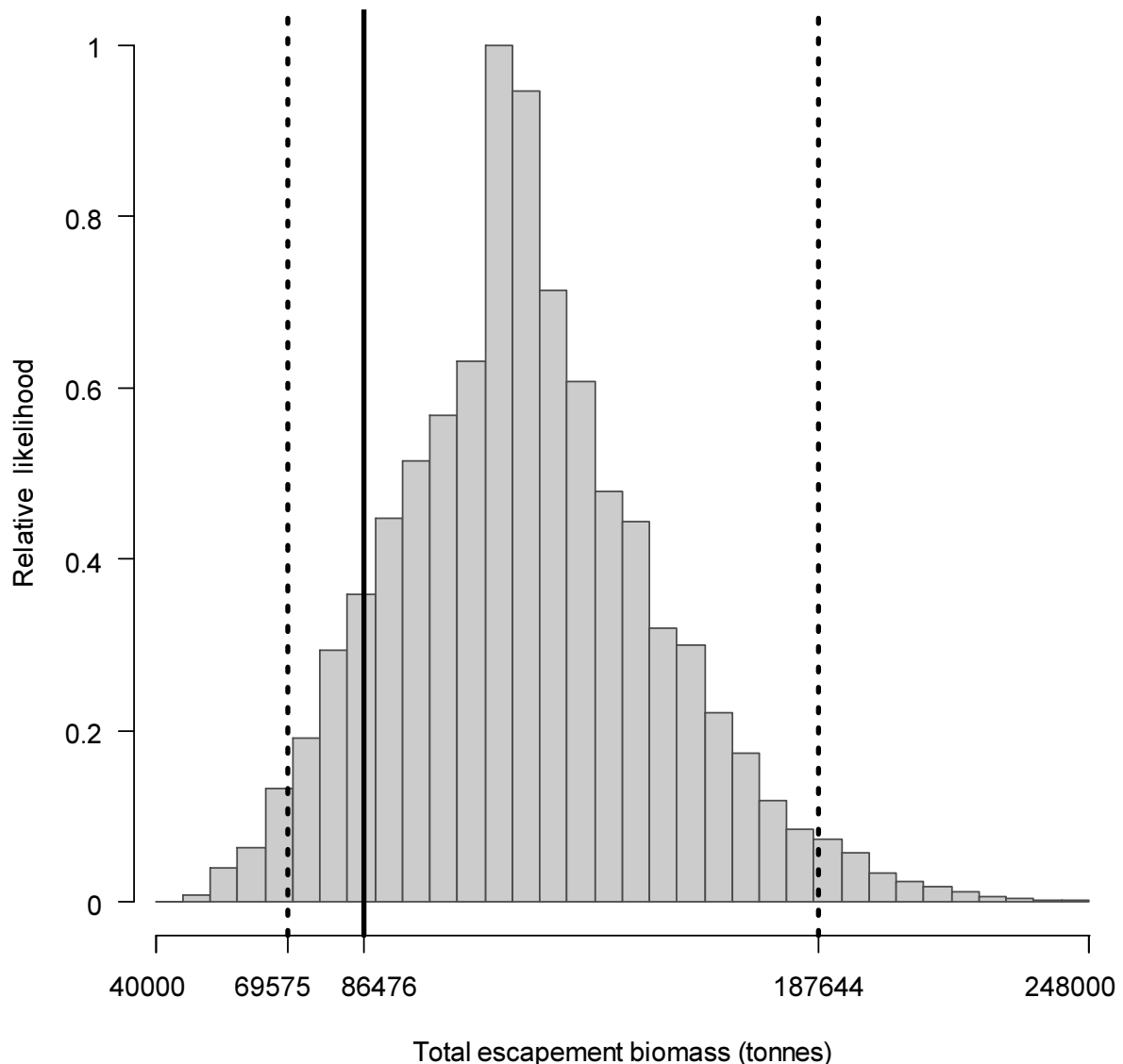
Figure 11 [previous page]. Likelihood distribution with 95% confidence intervals of total *D. gahi* escapement biomass at the season end (May 2nd).

Immigration

Doryteuthis gahi immigration during the season was inferred on each day by how many more squid were estimated present than the day before, minus the number caught and the number expected to have died naturally:

$$\text{Immigration } N_{day\ i} \quad = \quad N_{day\ i} - (N_{day\ i-1} - C_{day\ i-1} - M_{day\ i-1})$$

where $N_{day\ i-1}$ are optimized in the depletion models, $C_{day\ i-1}$ calculated as in Equation **3**, and $M_{day\ i-1}$ is:

$$M_{day\ i-1} \quad = \quad (N_{day\ i-1} - C_{day\ i-1}) \times (1 - e^{-M})$$

Immigration biomass per day was then calculated as the immigration number per day multiplied by predicted average individual weight from the GAM:

$$\text{Immigration } B_{day\ i} \quad = \quad \text{Immigration } N_{day\ i} \times {}_{GAM} Wt_{day\ i}$$

All numbers N are themselves derived from the daily average individual weights, therefore the estimation automatically factors in that those squid immigrating on a given day would likely be smaller than average (because younger). Confidence intervals of the immigration estimates were calculated by applying the above algorithms to the MCMC iterations of the depletion models. Resulting total biomasses of *D. gahi* immigration north and south, up to season end (day 122), were:

$$\text{Immigration } B_{S\ season} \quad = \quad 55{,}517 \text{ t} \sim 95\% \text{ CI } [24{,}429 \text{ to } 146{,}881] \text{ t} \qquad \textbf{(13-S)}$$

$$\text{Immigration } B_{N\ season} \quad = \quad 84{,}441 \text{ t} \sim 95\% \text{ CI } [39{,}505 \text{ to } 227{,}106] \text{ t} \qquad \textbf{(13-N)}$$

Total immigration with semi-randomized addition of the confidence intervals was:

$$\text{Immigration } B_{Total\ season} \quad = \quad 139{,}959 \text{ t} \sim 95\% \text{ CI } [98{,}376 \text{ to } 318{,}368] \text{ t} \qquad \textbf{(13-T)}$$

In the south sub-area, the in-season peaks on days 91, 95, and 104 accounted for approximately 40.6%, 21.6%, and 35.4% of in-season immigration (start day 55 was de facto not an in-season immigration), consistent with the variation in time series biomass on Figure 8. In the north sub-area, the in-season peaks on days 93, 101 and 111 accounted for approximately 9.8%, 14.0% and 14.6% of in-season immigration (Figure 10), while 60.6% was estimated present by the start of fishing on day 66, and therefore unknown to an actual immigration date.

Pinniped bycatch

Pinniped bycatch during 1st season 2019 totalled 7 reported fishing mortalities; 5 South American fur seals (*Arctocephalus australis*) and 2 Southern sea lions (*Otaria flavescens*),

distributed as summarized in Table 2 and Figure 12. The distribution of pinniped fishing mortalities was analysed for correlation with SEDs, aggregation by trawl and by vessel, daylight[b], position (latitude / longitude), trawl duration, and sea state. Correlations were tested by randomly re-distributing 100000× the pinniped mortalities among the 2685 commercial trawls during the season and calculating the proportions of the 100000 iterations that exceeded the empirical parameters[c]. The non-overlap between South American fur seal and Southern sea lion mortalities (Table 2) was also tested by these randomized re-distributions. All tests except non-overlap were calculated separately for the two pinniped species. Because the analysis implied multiple comparisons among stochastically independent null hypotheses, significance thresholds were adjusted by the Šidák correction:

$$\alpha_{corr} = 1 - (1 - \alpha)^{\frac{1}{m}} = 1 - (1 - 0.05)^{\frac{1}{5}} = 0.0102 \qquad \textbf{(14)}$$

where α = the standard significance threshold of p = 0.05, and m = number of independent null hypotheses: SED, daylight, position, duration, sea state; thus m = five[d]. The analysis was restricted to mortalities as live captures are ambiguous to quantify: escapees cannot be counted accurately and the same animals may be caught repeatedly (especially if they're habituated, therefore non-independence of counts).

Table 2. Reported fishing mortalities of pinnipeds, by trawl, in 1st season 2019.

Date	Species	No.	Grid at haul
Mar 15th	Southern sea lion	1	XPAP
Mar 15th	Southern sea lion	1	XQAP
Mar 25th	South American fur seal	1	XVAL
Mar 28th	South American fur seal	1	XVAL
Mar 28th	South American fur seal	1	XVAL
Mar 29th	South American fur seal	1	XVAL
Mar 29th	South American fur seal	1	XVAL

Results of the mortality analysis are summarized in Table 3. Pinniped mortalities were not aggregated by trawl as every South American fur seal and every Southern sea lion was reported killed in a different trawl. Pinniped mortalities were also not significantly aggregated by vessel as the five South American fur seals were taken on three different vessels (one vessel out of 16 took 3 and two other vessels took 1 each), and the two Southern sea lions were taken on two different vessels. 1048 of the 2685 commercial trawls were completed before SEDs were mandated on March 16th and March 29th. All pinniped mortalities occurred during this time; in trawls without SEDs. For South American fur seal mortalities, the 5/0 partition represented a statistically significant improvement of the subsequent use of SEDS. For Southern sea lion mortalities, the 2/0 partition was not statistically significant. As previously (e.g., Winter 2018b), significance of SED

---

[b] Daylight is defined as a trawl hauled between sunrise and sunset, calculated using the algorithms of the NOAA Earth System research laboratory, www.esrl.noaa.gov/gmd/grad/solcalc/calcdetails.html.
[c] Either counts or weighted means.
[d] Latitude and longitude, although computed separately, were considered part of the same position parameter, therefore only one null hypothesis including both. Aggregation of trawls and vessels were tested but unlike the other parameters are not potential causative agents of mortality, therefore not part of the same 'family' of null hypotheses. As vessels are nested within trawls there was also no separate 2-fold significance correction for trawl and vessel aggregation.

improvement is potentially biased because SED implementation was triggered by the precedence of mortalities, rather than assigned a priori, and therefore confounded with chronological progression as SEDs remained continually in use once they started to be used.
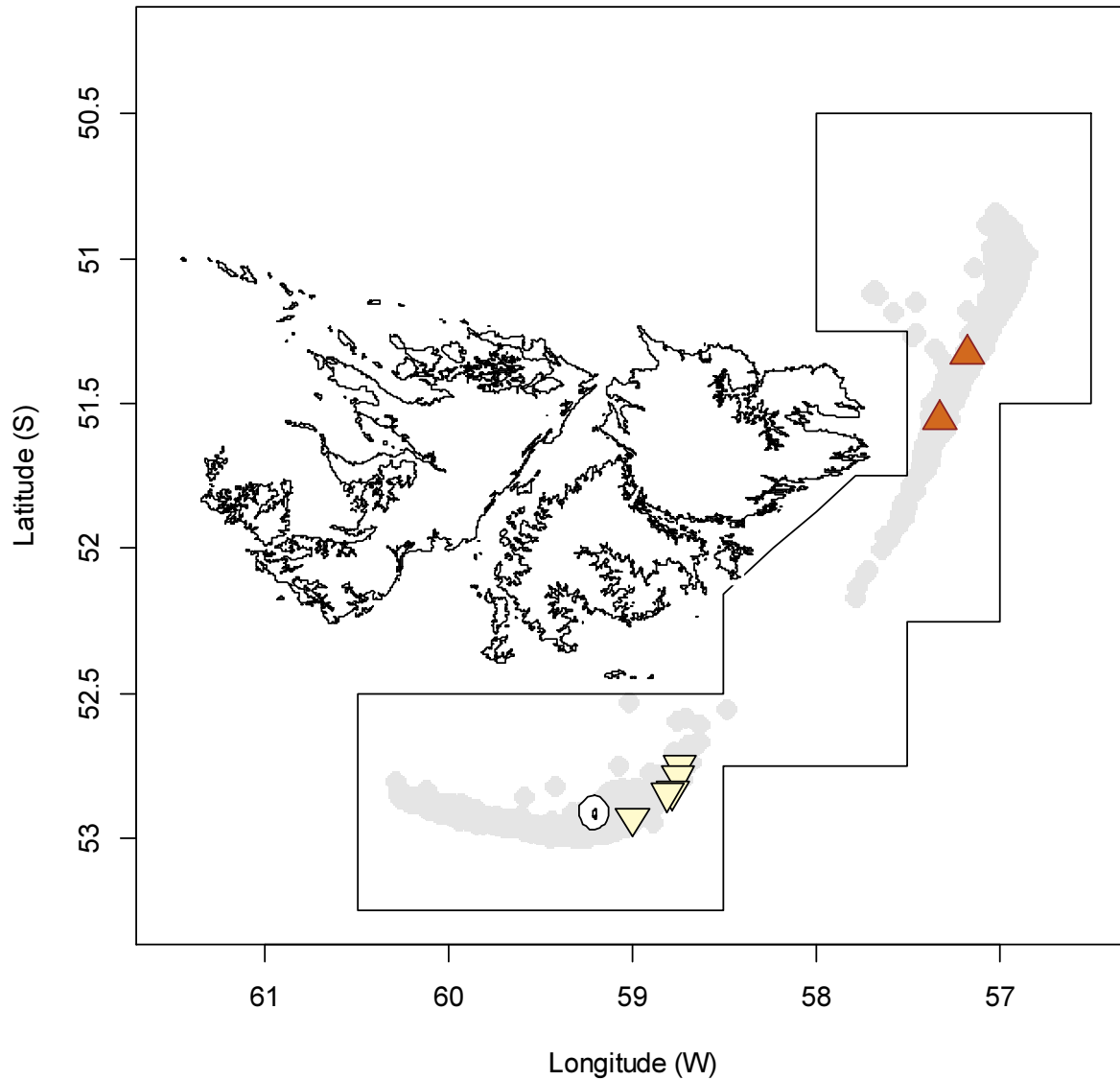

Figure 12. Distribution of pinniped trawl mortalities during the 1st season 2019. South American fur seals: off-white, point-down. Southern sea lions: brown, point-up. Grey under-shading: distribution of trawls, equivalent to Figure 3.

South American fur seal mortalities were clearly (Figure 12) and significantly (Table 3) clustered east of Beauchêne Island in the south of the Loligo Box. As in previous seasons (Winter 2017b, 2018a), Southern sea lion mortalities occurred further north (Figure 12), but spatial clustering of those two mortalities was not statistically significant (Table 3). The parameters of daylight, trawl duration, and sea state showed no significant correlation with either pinniped species mortality. The absence of overlap between South American fur seal and Southern sea lion mortalities (Table 2) was entirely non-significant, as given the relative scarcity of mortalities, >90% of randomizations showed no overlap either (Table 3).

Table 3. Hypotheses correlating pinniped mortalities in the 1st season 2019 commercial fishery. Outcomes are either the mortality counts or the mortality-weighted means of that hypothesis parameter. Non-significant parameters are shaded grey.

Mortality hypothesis	South American fur seal		Southern sea lion	
	Outcome	p	Outcome	p
Without SED	5 / 5	<0.0100	2 / 2	>0.1500
Trawl aggregation[a]	5 / 2685	1.0000	2 / 2685	1.0000
Vessel aggregation[b]	3 / 16	>0.0800	2 / 16	1.0000
Daylight	3 / 5	>0.0900	1 / 2	>0.2000
Lat / Lon position	52.83ºS × 58.81ºW	<0.0010	51.44ºS × 57.24ºW	>0.2000
Trawl duration	3.32 hours	>0.7000	4.13 hours	>0.3000
Sea state[c]	2.40	>0.8000	3.00	>0.5000
Both species				
Non-overlap	0 / 7	>0.9000	-	-

[a] See Table 2.
[b] Vessels not identified, for confidentiality.
[c] Beaufort wind force scale.

Fishery bycatch

Figure 13 [below]. Distributions of the eight principal bycatches during 1st season 2019, by noon position grids. Thickness of grid lines is proportional to the number of vessel-days (1 to 199 per grid; 20 different grids were occupied). Grey-scale is proportional to the bycatch biomass; maximum (tonnes) indicated on each plot.

Illex

Toothfish
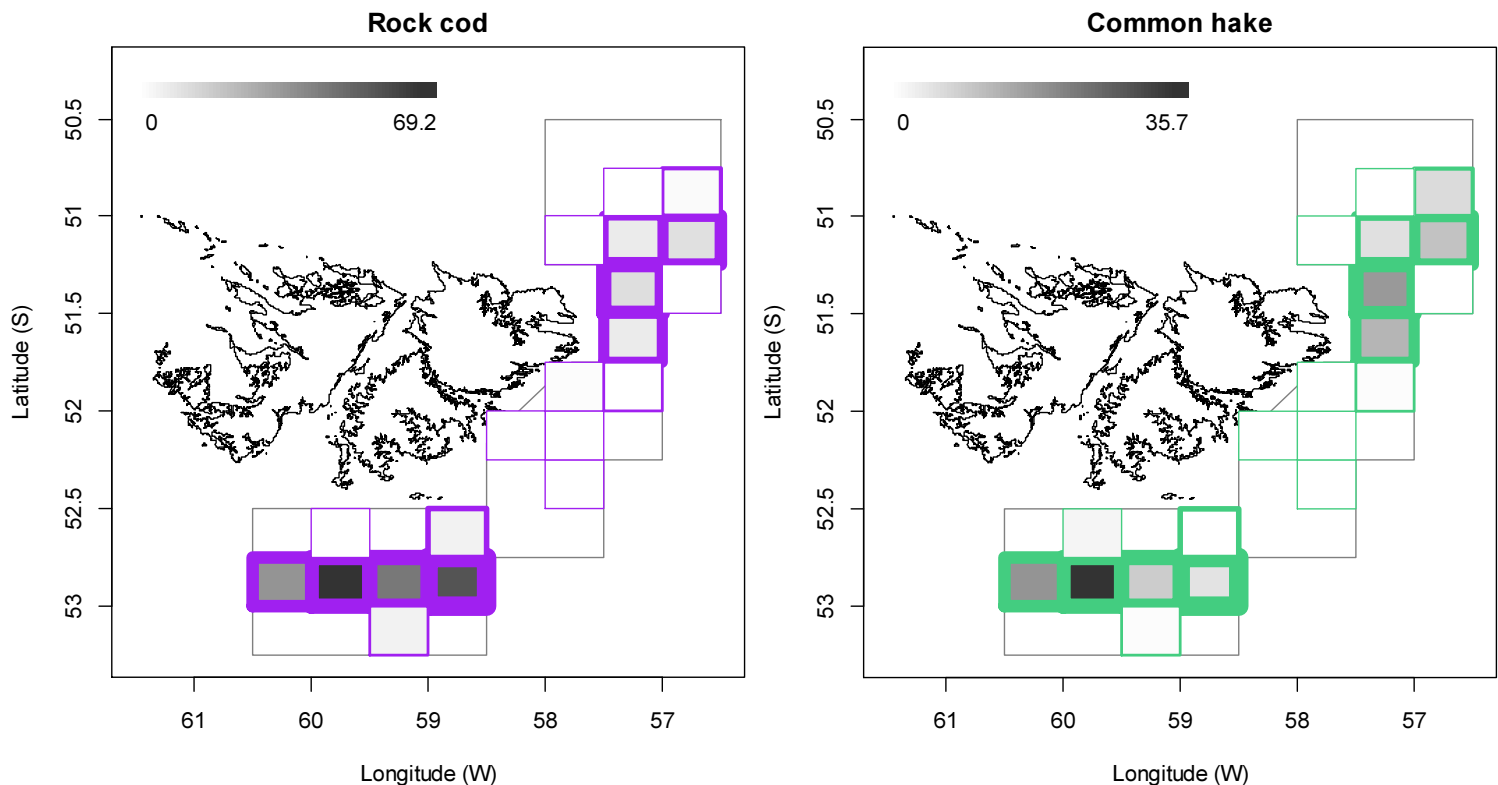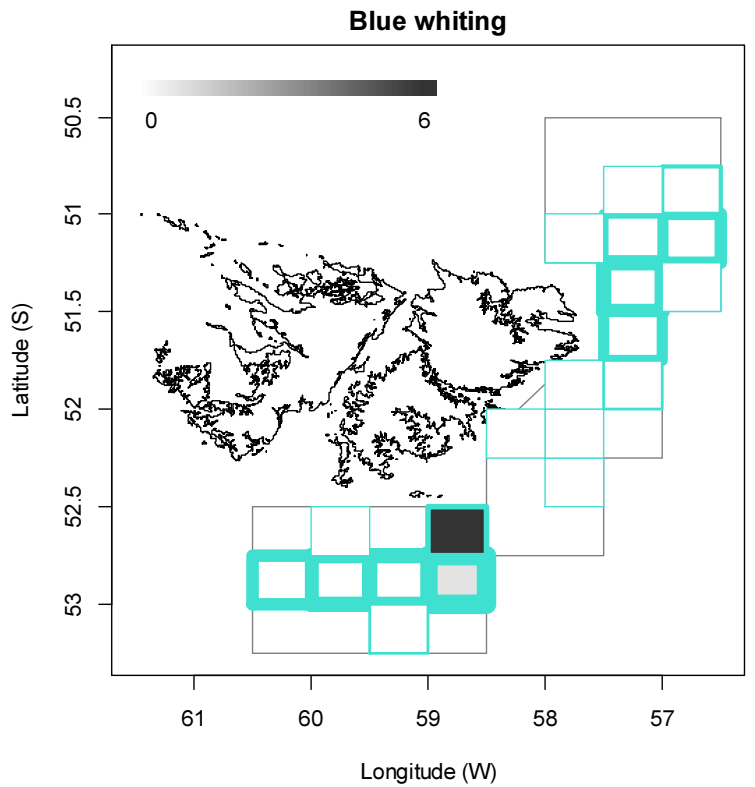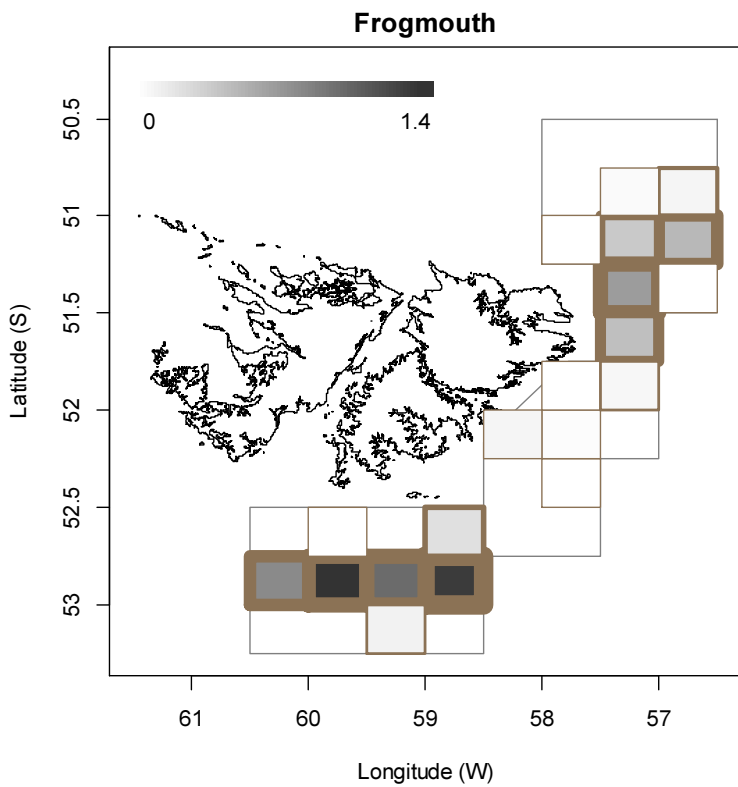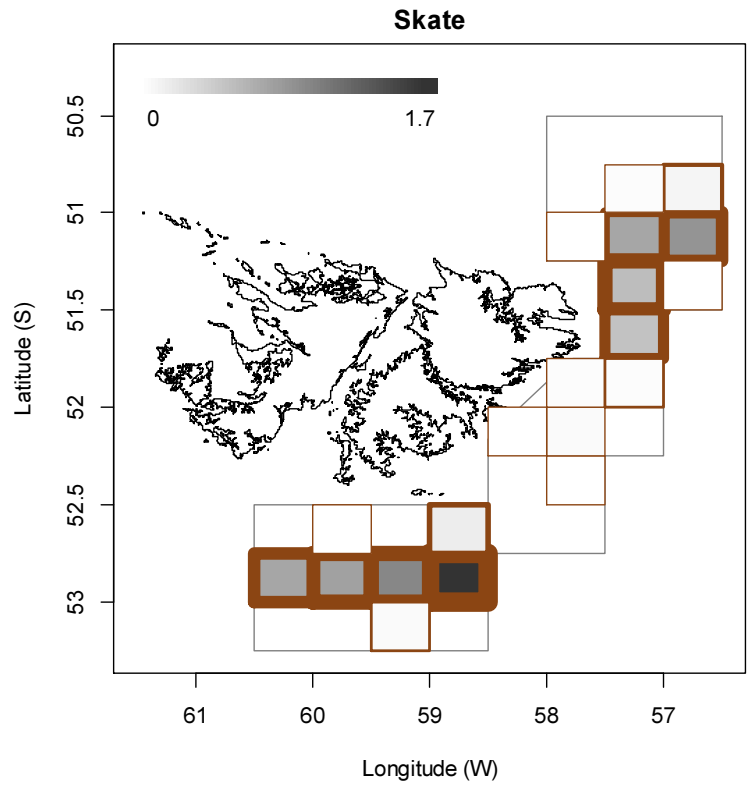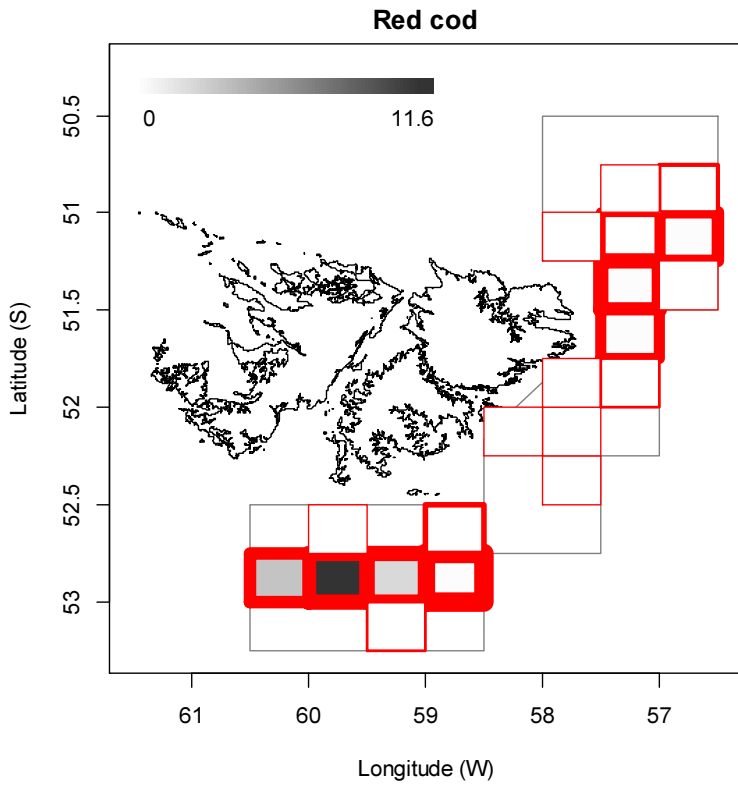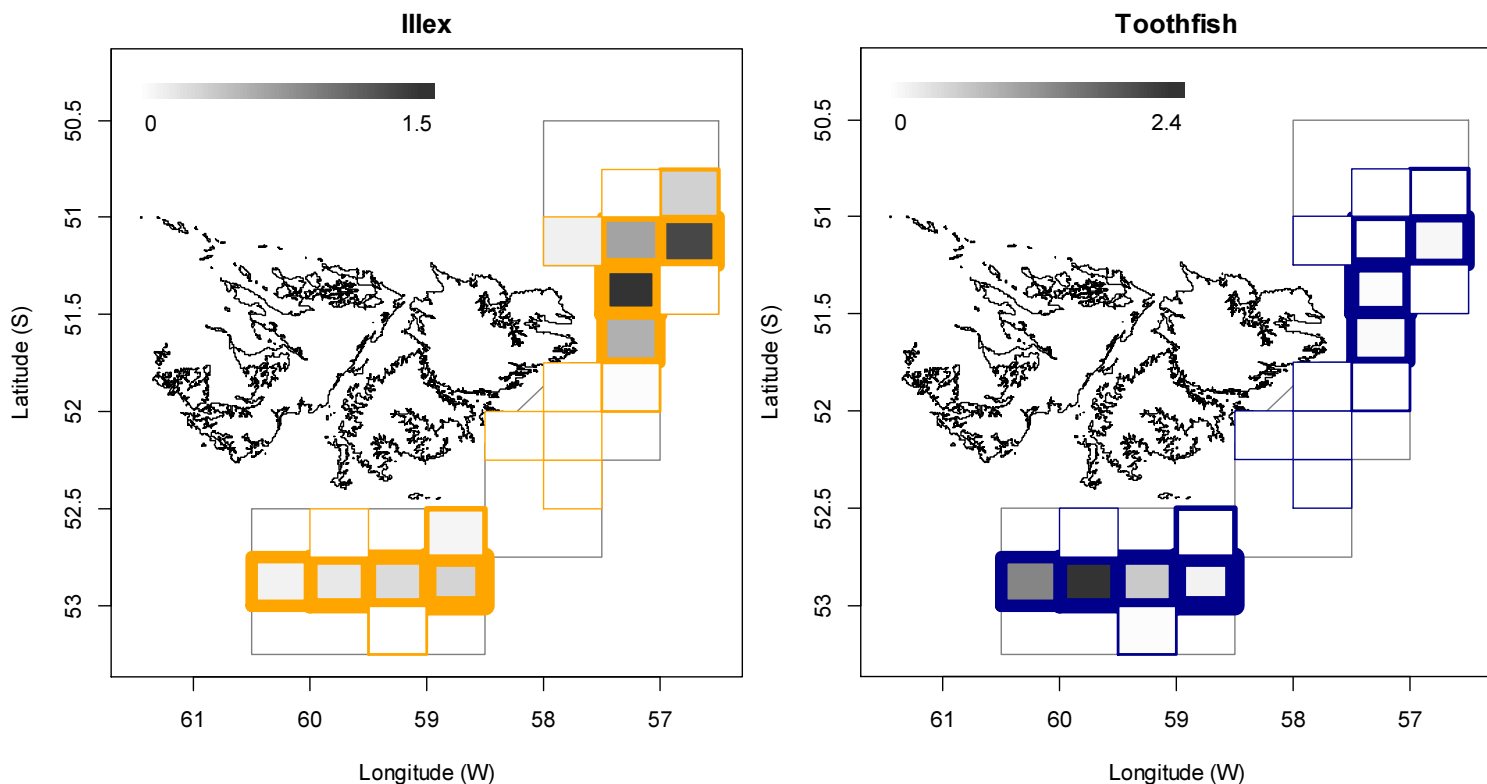
All of the 953 1st season vessel-days (Table 1) reported *D. gahi* squid as their primary catch. The proportion of total catch represented by *D. gahi* (55585600/56034376 = 0.992; Table A1) is the highest for a first season since 2005. Highest bycatches in 1st season 2019 were rock cod (*Patagonotothen ramsayi*), with 257 t from 880 vessel-days, common hake *Merluccius hubbsi* (124 t, 433 vessel-days), red cod *Salilota australis* (17 t, 171 vessel-days), skate Rajiformes (7 t, 401 vessel-days), frogmouth *Cottoperca gobio* (7 t, 393 vessel-days), blue whiting *Micromesistius australis* (7 t, 5 vessel-days), shortfin squid *Illex argentinus* (5 t, 267 vessel-days), and toothfish *Dissostichus eleginoides* (5 t, 214 vessel-days). Relative distributions by grid of these bycatches are shown in Figure 13, and the complete list of all catches by species is given in Table A1.

Trawl area coverage

The impact of bottom trawling on seafloor habitat has been a matter of concern in commercial fisheries (Kaiser et al. 2002; 2006), whereby the potential severity of impact relates to spatial and temporal extents of trawling (Piet and Hintzen 2012, Gerritsen et al. 2013). For the *D. gahi* fishery, available catch, effort, and positional data are used to summarize the estimated 'ground' area coverage occupied during the season of trawling.

The procedure for summarizing trawl area coverage is described in the Appendix. 50% of total *D. gahi* catch was taken from 1.0% of the total area of the Loligo Box, corresponding approximately[e] to the aggregate of grounds trawled ≥13.9 times. 90% of total *D. gahi* catch was taken from 3.9% of the total area of the Loligo Box, corresponding

---

[e] However, not exactly. There is an expected strong correlation between the density of *D. gahi* catch taken from area units and how often these area units were trawled, but the correlation is not perfectly monotonic.

approximately to the aggregate of grounds trawled ≥2.7 times. 100% of total *D. gahi* catch over the season was taken from 7.7% of the total area of the Loligo Box, obviously corresponding to the aggregate of all grounds trawled at least once (Figure 14 - left). Conversely, this means that 92.3% of the area of the Loligo Box was never trawled during the season. The 92.3% estimate should be seen with the caveat that it includes the sum of all patches of terrain, no matter how small, that escaped the criss-cross of trawl tracks, and not every patch of terrain is a valuable marine habitat reserve. Averaged by 5 × 5 km grid (Figure 14 - right), 3 grids (out of 1383) had coverage of 15 or more (that is to say, every patch of ground within that 5 × 5 km was on average trawled over 15 times or more). Forty-three grids had coverage of 5 or more, and 64 grids had coverage of 2 or more.

The 7.7% of Loligo Box area that accounted for total *D. gahi* catch is very similar to the 7.1% of area in 1st season 2018 (Winter 2018a); also a season of high catch. The steep curve of cumulative trawl tracks as well as the small proportion of area cover are consistent with conclusions that at high spatial resolution, trawl footprints are small in regions of sustainably managed fishing rates (Amoroso et al. 2018).
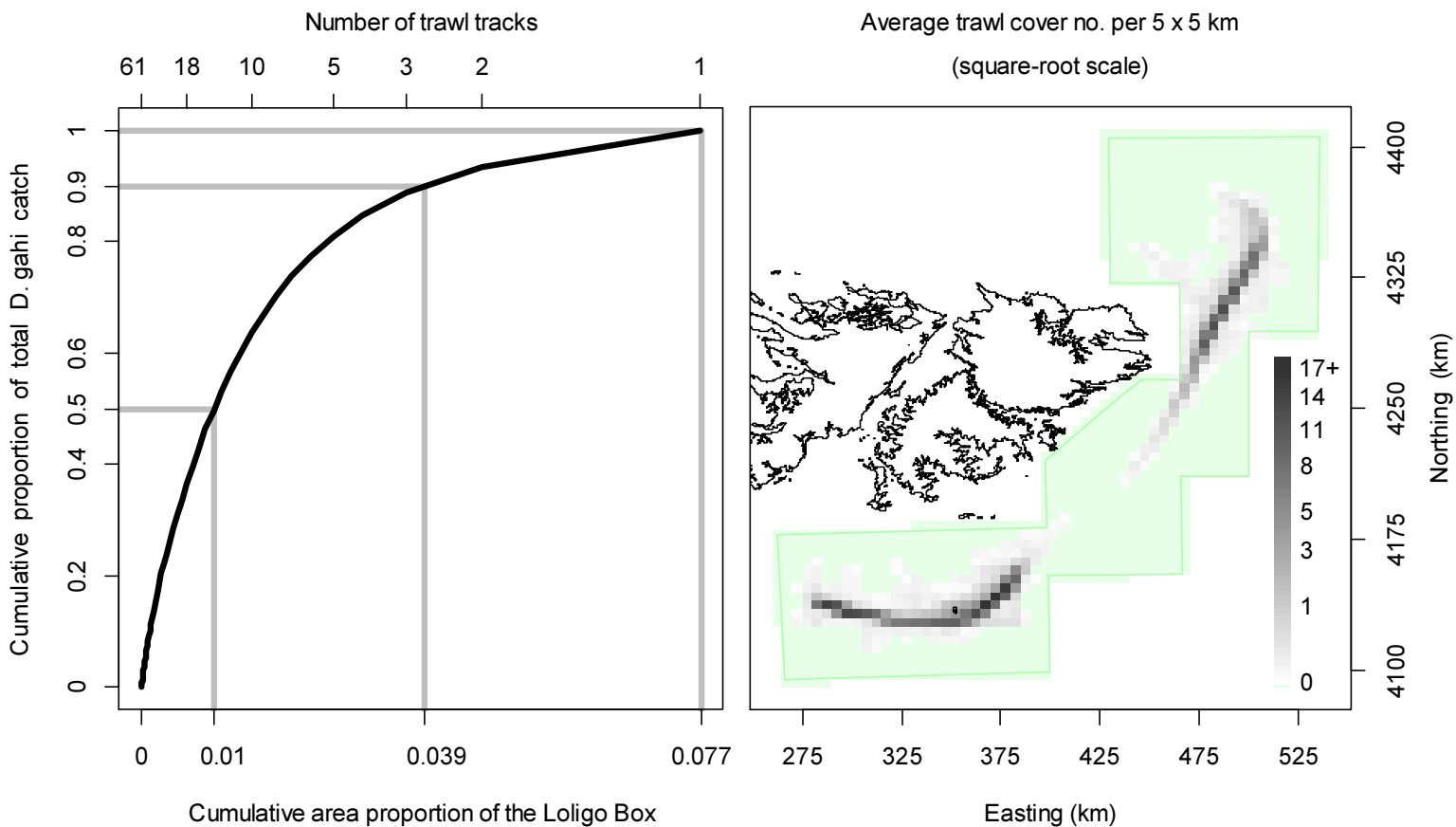
Figure 14. Left: cumulative *D. gahi* catch of 1st season 2019, vs. cumulative area proportion of the Loligo Box the catch was taken from. The maximum number of times that any single area unit was trawled was 61, and catch cumulation by reverse density corresponded approximately to the trawl multiples shown on the top x-axis. Right: trawl cover averaged by 5 × 5 km grid; green area represents zero trawling.

References

Agnew, D.J., Baranowski, R., Beddington, J.R., des Clers, S., Nolan, C.P. 1998. Approaches to assessing stocks of *Loligo gahi* around the Falkland Islands. Fisheries Research 35: 155-169.

Agnew, D. J., Beddington, J. R., and Hill, S. 2002. The potential use of environmental information to manage squid stocks. Canadian Journal of Fisheries and Aquatic Sciences, 59: 1851–1857.

Amoroso, R.O., Pitcher, C.R., Rijnsdorp, A.D., McConnaughey, R.A., Parma, A.M., Suuronen, P., Eigaard, O.R., Bastardie, F., Hintzen, N.T., Althaus, F., Baird, S.J., Black, J., Buhl-Mortensen, L., Campbell, A.B., Catarino, R., Collie, J., Cowan Jr., J.H., Durholtz, D., Engstrom, N., Fairweather, T.P., Fock, H.O., Ford, H., Gálvez, P.A., Gerritsen, H., Góngora, M.E., González, J.A., Hiddink, J.G., Hughes, K.M., Intelmann, S.S., Jenkins, C., Jonsson, P., Kainge, P., Kangas, M., Kathena, J.N., Kavadas, S., Leslie, R.W., Lewis, S.G., Lundy, M., Makin, D., Martin, J., Mazor, T., Gonzalez-Mirelis, G., Newman, S.J., Papadopoulou, N., Posen, P.E., Rochester, W., Russo, T, Sala, A., Semmen, J.M., Silva, C., Tsolos, A., Vanelslander, B., Wakefield, C.B., Wood, B.A., Hilborn, R., Kaiser, M.J., Jennings, S. 2018. Bottom trawl fishing footprints on the world's continental shelves. Proceedings of the National Academy of Science www.pnas.org/cgi/doi/10.1073/pnas.1802379115.

Arkhipkin, A. 1993. Statolith microstructure and maximum age of *Loligo gahi* (Myopsida: Loliginidae) on the Patagonian Shelf. Journal of the Marine Biological Association of the UK 73: 979-982.

Arkhipkin, A.I., Middleton, D.A.J. 2002. Sexual segregation in ontogenetic migrations by the squid *Loligo gahi* around the Falkland Islands. Bulletin of Marine Science 71: 109-127.

Arkhipkin, A.I., Middleton, D.A.J., Barton, J. 2008. Management and conservation of a short-lived fishery resource: *Loligo gahi* around the Falkland Islands. American Fisheries Society Symposium 49: 1243-1252.

Barton, J. 2002. Fisheries and fisheries management in Falkland Islands Conservation Zones. Aquatic Conservation: Marine and Freshwater Ecosystems 12: 127–135.

Brooks, S.P., Gelman, A. 1998. General methods for monitoring convergence of iterative simulations. Journal of computational and graphical statistics 7:434-455.

Chen, X., Chen, Y., Tian, S., Liu, B., Qian, W. 2008. An assessment of the west winter-spring cohort of neon flying squid (*Ommastrephes bartramii*) in the Northwest Pacific Ocean. Fisheries Research 92: 221-230.

DeLury, D.B. 1947. On the estimation of biological populations. Biometrics 3: 145-167.

Doubleday, Z.A., Prowse, T.A.A., Arkhipkin, A., Pierce, G.J., Semmens, J., Steer, M., Leporati, S.C., Lourenço, S., Quetglas, A., Sauer, W., Gillanders, B.M. 2016. Global proliferation of cephalopods. Current Biology 26: R387-R407.

Gamerman, D., Lopes, H.F. 2006. Markov Chain Monte Carlo. Stochastic simulation for Bayesian inference. 2nd edition. Chapman & Hall/CRC.

Gerritsen, H.D., Minto, C., Lordan, C. 2013. How much of the seabed is impacted by mobile fishing gear? Absolute estimates from Vessel Monitoring System (VMS) point data. ICES Journal of Marine Science 70: 523-531.

Hall, J. 2019. Observer Report 1230. Technical Document, FIG Fisheries Department. 31 p.

Hoenig, J.M. 1983. Empirical use of longevity data to estimate mortality rates. Fishery Bulletin 82: 898-903.

Jiao, Y., Cortés, E., Andrews, K., Guo, F. 2011. Poor-data and data-poor species stock assessment using a Bayesian hierarchical approach. Ecological Applications 21: 2691-2708.

Kaiser, M.J., Collie, J.S., Hall, S.J., Jennings, S., Poiner, I.R. 2002. Modification of marine habitats by trawling activities: prognosis and solutions. Fish and Fisheries 3: 114-136.

Kaiser, M.J., Clarke, K.R., Hinz, H., Austen, M.C.V., Somerfield, P.J., Karakassis, I. 2006. Global analysis of response and recovery of benthic biota to fishing. Marine Ecology Progress Series 311: 1-14.

Keller, S., Robin, J.P., Valls, M., Gras, M., Cabanellas-Reboredo, M., Quetglas, A. 2015. The use of depletion models to assess Mediterranean cephalopod stocks under the current EU data collection framework. Mediterranean Marine Science 16: 513-523.

Magnusson, A., Punt, A., Hilborn, R. 2013. Measuring uncertainty in fisheries stock assessment: the delta method, bootstrap, and MCMC. Fish and Fisheries 14: 325-342.

Medellín-Ortiz, A., Cadena-Cárdenas, L., Santana-Morales, O. 2016. Environmental effects on the jumbo squid fishery along Baja California's west coast. Fisheries Science 82: 851-861.

Morales-Bojórquez, E., Hernández-Herrera, A., Cisneros-Mata, M.A., Nevárez-Martínez, M.O. 2008. Improving estimates of recruitment and catchability of jumbo squid *Dosidicus gigas* in the Gulf of California, Mexico. Journal of Shellfish Research 27: 1233-1237.

Nash, J.C., Varadhan, R. 2011. optimx: A replacement and extension of the optim() function. R package version 2011-2.27. http://CRAN.R-project.org/package=optimx

Patterson, K.R. 1988. Life history of Patagonian squid *Loligo gahi* and growth parameter estimates using least-squares fits to linear and von Bertalanffy models. Marine Ecology Progress Series 47: 65-74.

Payá, I. 2010. Fishery Report. *Loligo gahi*, Second Season 2009. Fishery statistics, biological trends, stock assessment and risk analysis. Technical Document, Falkland Islands Fisheries Dept. 54 p.

Pebesma, E., Bivand, R., Rowlingson, B., Gomez-Rubio, V., Hijmans, R., Sumner, M., MacQueen, D., Lemon, J., O'Brien, J., O'Rourke, J. 2018. Package 'sp'. Classes and Methods for Spatial Data. Version 1.3-1. https://cran.r-project.org/web/packages/sp/index.html.

Pierce, G.J., Guerra, A. 1994. Stock assessment methods used for cephalopod fisheries. Fisheries Research 21: 255 – 285.

Piet, G.J., Hintzen, N.T. 2012. Indicators of fishing pressure and seafloor integrity. ICES Journal of Marine Science 69: 1850-1858.

Punt, A.E., Hilborn, R. 1997. Fisheries stock assessment and decision analysis: the Bayesian approach. Reviews in Fish Biology and Fisheries 7:35-63.

Roa-Ureta, R. 2012. Modelling in-season pulses of recruitment and hyperstability-hyperdepletion in the *Loligo gahi* fishery around the Falkland Islands with generalized depletion models. ICES Journal of Marine Science 69: 1403–1415.

Roa-Ureta, R., Arkhipkin, A.I. 2007. Short-term stock assessment of *Loligo gahi* at the Falkland Islands: sequential use of stochastic biomass projection and stock depletion models. ICES Journal of Marine Science 64: 3-17.

Roberts, G. 2019. Observer Report 1226. Technical Document, FIG Fisheries Department. 35 p.

Rosenberg, A.A., Kirkwood, G.P., Crombie, J.A., Beddington, J.R. 1990. The assessment of stocks of annual squid species. Fisheries Research 8: 335-350.

Royer, J., Périès, P., Robin, J.P. 2002. Stock assessments of English Channel loliginid squids: updated depletion methods and new analytical methods. ICES Journal of Marine Science 59: 445-457.

Shaw, P.W., Arkhipkin, A.I., Adcock, G.J., Burnett, W.J., Carvalho, G.R., Scherbich, J.N., Villegas, P.A. 2004. DNA markers indicate that distinct spawning cohorts and aggregations of Patagonian squid, *Loligo gahi*, do not represent genetically discrete subpopulations. Marine Biology, 144: 961-970.

Su, Z., Adkison, M.D., Van Alen, B.W. 2001. A hierarchical Bayesian model for estimating historical salmon escapement and escapement timing. Canadian Journal of Fisheries and Aquatic Sciences 58: 1648-1662.

Swartzman, G., Huang, C., Kaluzny, S. 1992. Spatial analysis of Bering Sea groundfish survey data using generalized additive models. Canadian Journal of Fisheries and Aquatic Sciences 49: 1366-1378.

Tutjavi, V. 2019. Observer Report 1225. Technical Document, FIG Fisheries Department. 23 p.

Winter, A. 2014. *Loligo* stock assessment, second season 2014. Technical Document, Falkland Islands Fisheries Department. 30 p.

Winter, A. 2017a. Stock assessment – Falkland calamari (*Doryteuthis gahi*). Technical Document, Falkland Islands Fisheries Department. 30 p.

Winter, A. 2017b. Stock assessment – *Doryteuthis gahi* 2nd season 2017. Technical Document, Falkland Islands Fisheries Department. 37 p.

Winter, A. 2018a. Stock assessment – *Doryteuthis gahi* 1st season 2018. Technical Document, Falkland Islands Fisheries Department. 36 p.

Winter, A. 2018b. Stock assessment – *Doryteuthis gahi* 2nd season 2018. Technical Document, Falkland Islands Fisheries Department. 34 p.

Winter, A., Arkhipkin, A. 2015. Environmental impacts on recruitment migrations of Patagonian longfin squid (*Doryteuthis gahi*) in the Falkland Islands with reference to stock assessment. Fisheries Research 172: 85-95.

Winter, A., Zawadowski, T. Tutjavi, V. 2019. *Doryteuthis gahi* stock assessment survey, 1st season 2019. Technical Document, Falkland Islands Fisheries Department. 18 p.

Young, I.A.G., Pierce, G.J., Daly, H.I., Santos, M.B., Key, L.N., Bailey, N., Robin, J.-P., Bishop, A.J., Stowasser, G., Nyegaard, M., Cho, S.K., Rasero, M., Pereira, J.M.F. 2004. Application of depletion methods to estimate stock size in the squid *Loligo forbesi* in Scottish waters (UK). Fisheries Research 69: 211-227.
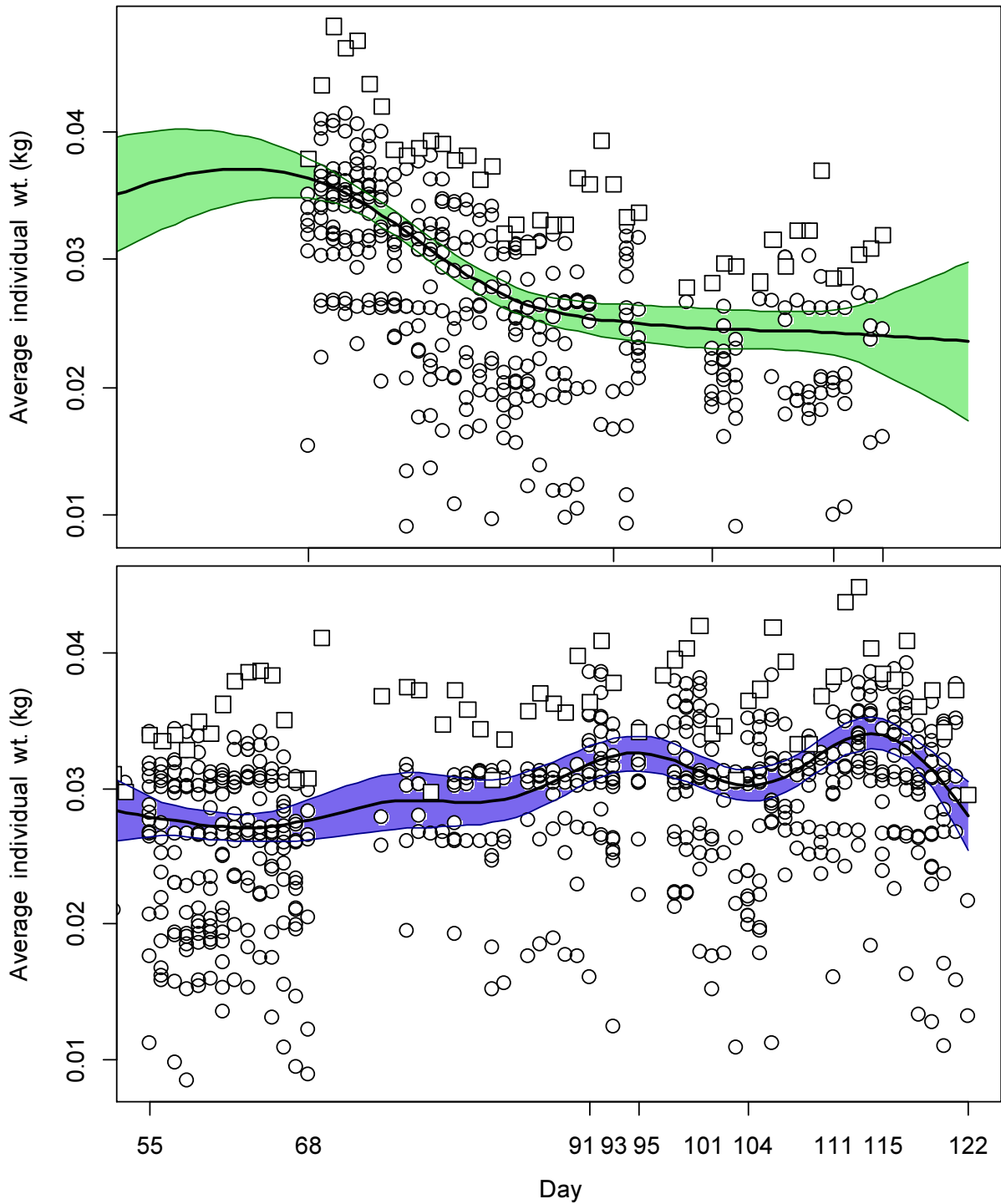
Figure A1. North (top) and south (bottom) sub-area daily average individual *D. gahi* weights from commercial size categories per vessel (circles) and observer measurements (squares). GAMs of the daily trends ± 95% confidence intervals (centre lines and colour under-shading).

To smooth fluctuations, GAM trends were calculated of daily average individual weights. North and south sub-areas were calculated separately. For continuity, GAMs were calculated

using all pre-season survey and in-season data contiguously. North and south GAMs were first calculated separately on the commercial and observer data. Commercial data GAMs were taken as the baseline trends, and calibrated to observer data GAMs in proportion to the correlation between commercial data and observer data GAMs. For example, if the season average individual weight estimate from commercial data was 0.052 kg, the season average individual weight estimate from observer data was 0.060 kg, and the coefficient of determination (R^2) between commercial and observer GAM trends was 86%, then the resulting trend of daily average individual weights was calculated as the commercial data GAM values + $(0.060 - 0.052) \times 0.86$. This way, both the greater day-to-day consistency of the commercial data trends, and the greater point value accuracy of the observer data are represented in the calculations. GAM plots of the north and south sub-areas are in Figure A1.

Prior estimates and CV

The pre-season survey had estimated *D. gahi* biomasses of 44,998 t south of 52° S and 4620 t north of 52° S (Winter et al. 2019). As catches per effort in the north started off high on day 68 (March 9th) (Figures 4 and 6), further immigration of *D. gahi* must have occurred in the north between the end of the survey and day 68. Accordingly, catchability (q) based on the survey biomass estimate was not applicable as a depletion model prior for the north. Instead, the same q prior as the south was used, from the principle that in a Bayesian analysis unavailable prior data values can be 'borrowed' from comparable data sets (Su et al. 2001, Jiao et al 2011). This approach has previously been implemented in the 1st season 2017 stock assessment (Winter 2017a). Hierarchical bootstrapping of the inverse distance weighting algorithm obtained a coefficient of variation (CV) of 13.0% of the survey biomass distributions. From modelled survey catchability, Payá (2010) had estimated average net escapement of up to 22%, which was added to the CV:

$$44{,}998 \pm (.130 + .22) = 44{,}998 \pm 35.0\% \quad = \quad 44{,}998 \pm 15{,}766 \text{ t} \qquad \textbf{(A1-S)}$$

$$4{,}620 \pm (.130 + .22) = 4{,}620 \pm 35.0\% \quad = \quad 4{,}620 \pm 1{,}619 \text{ t} \qquad \textbf{(A1-N)}$$

The 22% escapement was added as a linear increase in the variability, but was not used to reduce the total estimate, because squid that escape one trawl are likely to be part of the biomass concentration that is available to the next trawl.

    D. gahi numbers at the end of the survey were estimated as the survey biomasses divided by the GAM-predicted individual weight averages for the survey: 0.0296 kg south, 0.0314 kg north (Figure A1), and 0.0305 kg combined. Average coefficients of variation (CV) of the GAM over the duration of the pre-season survey were 5.5% south and 8.8% north. CV of the length-weight conversion relationship (Equation **8**) were 7.7% south and 6.9% north. Joining these sources of variation with the pre-season survey biomass estimates and individual weight averages (above) gave estimated *D. gahi* numbers at survey end (day 53) of:

$$\text{prior } N_{\text{S day 53}} \quad = \quad \frac{44{,}998 \times 1000}{0.0296} \pm \sqrt{35.0\%^2 + 5.5\%^2 + 7.7\%^2}$$

$$= \quad 1.522 \times 10^9 \pm 36.3\%$$

$$\text{prior } N_{\text{N day 53}} \quad = \quad \frac{4620 \times 1000}{0.0305} \pm \sqrt{35.0\%^2 + 8.8\%^2 + 6.9\%^2}$$

$$= 1.470 \times 10^9 \pm 36.8\%$$

Priors were normalized for the combined fishing zone average, to produce better continuity as vessels cross back and forth between north and south:

$$\text{nprior } N_{\text{S day 53}} = \left(\frac{(44{,}998 + 4620) \times 1000}{0.0305}\right) \times \left(\frac{\text{prior} N_{\text{S day 53}}}{\text{prior} N_{\text{N day 53}} + \text{prior} N_{\text{S day 53}}}\right)$$

$$= 1.483 \times 10^9 \pm 36.3\% \tag{A2-S}$$

The catchability coefficient (q) prior for the south sub-area was taken on day 55, the first day of the season, when 15 vessels fished in the south and the initial depletion period south started. Abundance on day 55 was discounted for natural mortality over the 2 days since the end of the survey:

$$\text{nprior } N_{\text{S day 55}} = \text{nprior } N_{\text{S day 53}} \times e^{-M \cdot (55-53)} - \text{CNMD}_{\text{S day 55}} = 1.444 \times 10^9 \tag{A3-S}$$

where $\text{CNMD}_{\text{S day 55}} = 0$ as no catches intervened between the end of the survey and the start of commercial season. Thus:

$$\text{prior } q_S = C(N)_{\text{S day 55}} / (\text{nprior } N_{\text{S day 55}} \times E_{\text{S day 55}})$$

$$= (C(B)_{\text{S day 55}} / Wt_{\text{S day 55}}) / (\text{nprior } N_{\text{S day 55}} \times E_{\text{S day 55}})$$

$$= (991.8 \text{ t} / 0.027925 \text{ kg}) / (1.444 \times 10^9 \times 15 \text{ vessel-days})$$

$$= 1.640 \times 10^{-3} \text{ vessels}^{-1 \text{ f}} \tag{A4-S}$$

CV of the prior was calculated as the sum of variability in $\text{nprior } N_{\text{S day 53}}$ (Equation **A2-S**) plus variability in the catches of vessels on start day 55, plus variability of the natural mortality (see Appendix section Natural mortality, below):

$$CV_{\text{prior S}} =$$

$$\sqrt{36.3\%^2 + \left(\frac{SD\left(C(B)_{\text{S vessels day 55}}\right)}{\text{mean}\left(C(B)_{\text{S vessels day 55}}\right)}\right)^2 + (1 - \text{sign}(1 - CV_M) \times \text{abs}(1 - CV_M)^{(55-53)})^2}$$

$$= \sqrt{36.3\%^2 + 21.0\%^2 + 28.5\%^2} \qquad = 50.7\% \tag{A5-S}$$

The catchability coefficient (q) prior for the north sub-area was, as noted, taken to be the same as the south sub-area:

$$\text{prior } q_N = \text{prior } q_S = 1.640 \times 10^{-3} \text{ vessels}^{-1 \text{ g}} \tag{A4-N}$$

---

[f] On Figure 7-left.
[g] On Figure 9-left.

However, the coefficient of variation was augmented by the increased number of days of cumulative mortality in the north:

$$CV_{\text{prior N}} =$$

$$\sqrt{36.3\%^2 + \left(\frac{SD\left(C(B)_{\text{S vessels day 55}}\right)}{\text{mean}\left(C(B)_{\text{S vessels day 55}}\right)}\right)^2 + (1 - \text{sign}(1 - CV_M) \times \text{abs}(1 - CV_M)^{(68-53)})^2}$$

$$= \sqrt{36.3\%^2 + 21.0\%^2 + 91.9\%^2} \qquad = 101.0\% \qquad \textbf{(A5-N)}$$

Depletion model estimates and CV

For the south sub-area, the equivalent of Equation **3** with four N_{day} was optimized on the difference between predicted and actual catches (Equation **4**), resulting in parameters values:

depletion $N1_{\text{S day 55}}$ $= 3.781 \times 10^9$;   depletion $N2_{\text{S day 91}}$ $= 1.155 \times 10^9$
depletion $N3_{\text{S day 95}}$ $= 0.569 \times 10^9$;   depletion $N4_{\text{S day 104}}$ $= 0.930 \times 10^9$

depletion $q_{\text{S NSED}}$ $= 0.702 \times 10^{-3}$ [h]
depletion $q_{\text{S SED}}$ $= 0.564 \times 10^{-3}$ **(A6-S)**

The normalized root-mean-square deviation of predicted vs. actual catches was calculated as the CV of the model:

$$CV_{\text{rmsd S}} \quad = \quad \frac{\sqrt{\sum_{i=1}^{n}\left(_{\text{predicted}}C(N)_{\text{S day i}} - _{\text{actual}}C(N)_{\text{S day i}}\right)^2 / n}}{\text{mean}\left(_{\text{actual}}C(N)_{\text{S day i}}\right)}$$

$$= 2.459 \times 10^6 / 16.970 \times 10^6 = 14.5\% \qquad \textbf{(A7-S)}$$

$CV_{\text{rmsd S}}$ was added to the variability of the GAM-predicted individual weight averages for the season (Figure A1-S); equal to a CV of 2.25% south. CVs of the depletion were then calculated as the sum:

$$CV_{\text{depletion S}} \quad = \quad \sqrt{CV_{\text{rmsd S}}^2 + CV_{\text{GAM Wt S}}^2} \quad = \quad \sqrt{14.5\%^2 + 2.25\%^2}$$

$$= \quad 14.6\% \qquad \textbf{(A8-S)}$$

For the north sub-area, the Equation **3** equivalent with 4 N_{day} was optimized on the difference between predicted catches and actual catches (Equation **4**), resulting in parameters values:

depletion $N1_{\text{N day 68}}$ $= 7.403 \times 10^9$;   depletion $N2_{\text{N day 93}}$ $= 0.713 \times 10^9$
depletion $N3_{\text{N day 101}}$ $= 1.398 \times 10^9$;   depletion $N2_{\text{N day 111}}$ $= 1.485 \times 10^9$

depletion $q_{\text{N NSED}}$ $= 0.320 \times 10^{-3}$ [i]
depletion $q_{\text{N SED}}$ $= 0.314 \times 10^{-3}$ **(A6-N)**

---

[h] On Figure 7-left.
[i] On Figure 9-left.

The root-mean-square deviation of predicted vs. actual catches was calculated as the CV of the model:

$$CV_{rmsd\ N} = \frac{\sqrt{\sum_{i=1}^{n}\left(_{predicted}C(N)_{N\ day\ i} - _{actual}C(N)_{N\ day\ i}\right)^2 / n}}{mean\left(_{actual}C(N)_{N\ day\ i}\right)}$$

$$= 2.332 \times 10^6 / 11.651 \times 10^6 = 20.0\% \qquad \textbf{(A7-N)}$$

$CV_{rmsd\ N}$ was added to the variability of the GAM-predicted individual weight averages for the season (Figure A1-N); equal to a CV of 2.5% north. CVs of the depletion were then calculated as the sum:

$$CV_{depletion\ N} = \sqrt{CV_{rmsd\ N}^2 + CV_{GAM\ Wt\ N}^2} = \sqrt{20.0\%^2 + 2.5\%^2}$$

$$= 20.2\% \qquad \textbf{(A8-N)}$$

Combined Bayesian models

For the south sub-area, the joint optimization of Equations **4** and **5** resulted in parameters values:

Bayesian $N1_{S\ day\ 55}$	$= 2.425 \times 10^9$;	Bayesian $N2_{S\ day\ 91}$	$= 0.732 \times 10^9$
Bayesian $N3_{S\ day\ 95}$	$= 0.379 \times 10^9$;	Bayesian $N4_{S\ day\ 104}$	$= 0.671 \times 10^9$
Bayesian $q_{S\ NSED}$	$= 1.182 \times 10^{-3}$ [j]		
Bayesian $q_{S\ SED}$	$= 0.960 \times 10^{-3}$		**(A9-S)**

These parameters produced the fit between predicted catches and actual catches shown in Figure A2-S.

For the north sub-area, joint optimization of Equations **4** and **5** resulted in parameters values:

Bayesian $N1_{N\ day\ 68}$	$= 2.641 \times 10^9$;	Bayesian $N2_{N\ day\ 93}$	$= 0.332 \times 10^9$
Bayesian $N3_{N\ day\ 101}$	$= 0.486 \times 10^9$;	Bayesian $N4_{N\ day\ 111}$	$= 0.517 \times 10^9$
Bayesian $q_{N\ NSED}$	$= 0.925 \times 10^{-3}$ [k]		
Bayesian $q_{N\ SED}$	$= 0.990 \times 10^{-3}$		**(A9-N)**

These parameters produced the fit between predicted catches and actual catches shown in Figure A2-N.

Figure A2-S [next page]. Daily catch numbers estimated from actual catch (black points: without SEDs, black triangles: with SEDs) and predicted from the depletion model (purple line) in the south sub-area.

---

[j] On Figure 7-left.
[k] On Figure 9-left.

**South, four depletion peaks**

North, four depletion peaks
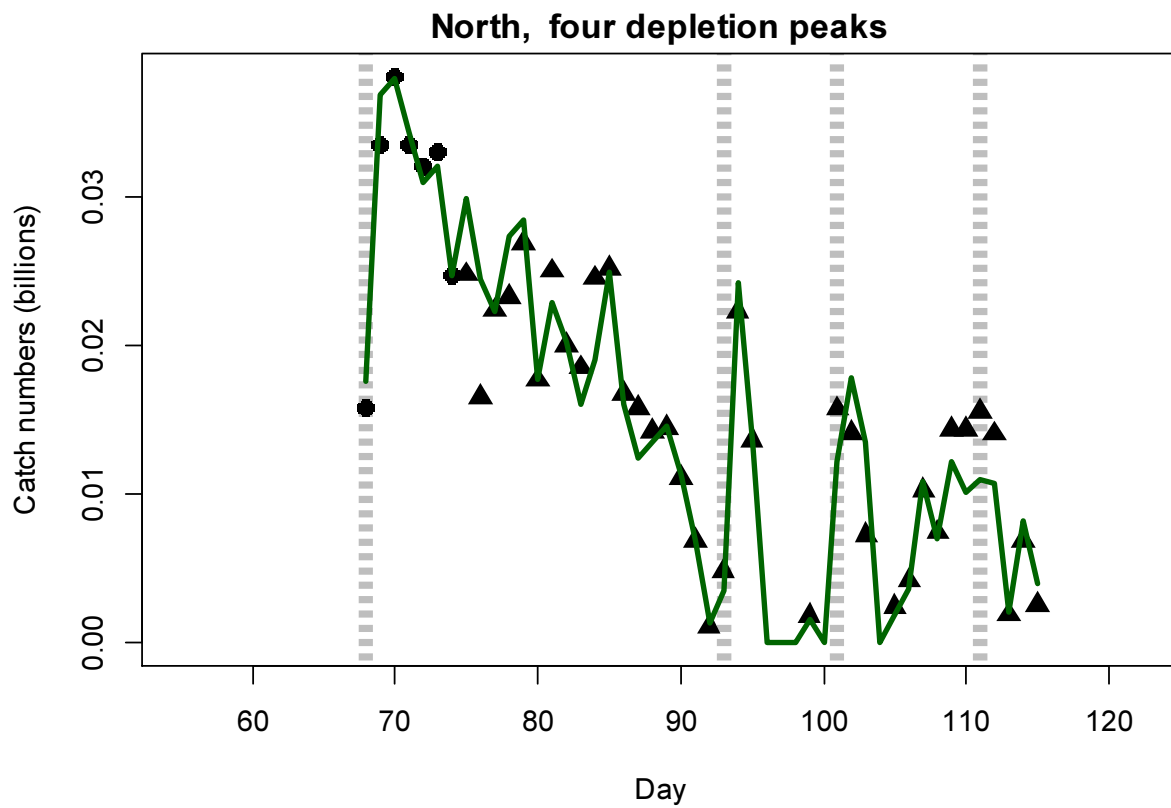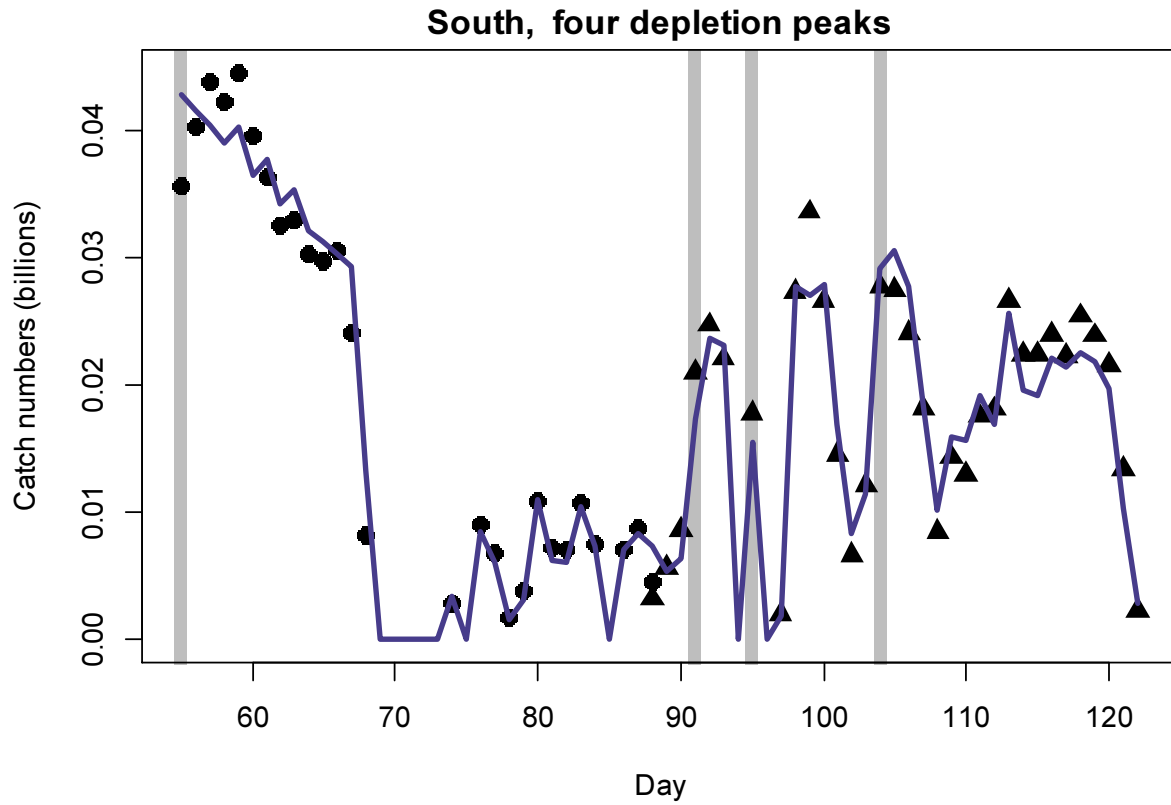
Figure A2-N. Daily catch numbers estimated from actual catch (black points: without SEDs, black triangles: with SEDs) and predicted from the depletion model (green line) in the north sub-area.

Natural mortality

Natural mortality is parameterized as a constant instantaneous rate M = 0.0133 day^{-1} (Roa-Ureta and Arkhipkin 2007), based on Hoenig's (1983) log mortality vs. log maximum age regression applied to an estimated maximum age of 352 days for *Doryteuthis gahi*:

$$\log (M) \qquad = \qquad 1.44 - 0.982 \times \log (age_{max})$$

$$M \qquad = \qquad \exp (1.44 - 0.982 \times \log (352))$$

$$= \qquad 0.0133 \qquad\qquad\qquad \textbf{(A10)}$$

Hoenig (1983) derived Equation **A10** from the regression of 134 stocks among 79 species of fish, molluscs, and cetaceans. Hoenig's regression obtained R^2 = 0.82, but a corresponding coefficient of variation (CV) was not published. An approximate CV of M was estimated by measuring the coordinates off a print of Figure 1 in Hoenig (1983) and repeating the regression. Variability of M was calculated by randomly re-sampling, with replacement, the regression coordinates 10000× and re-computing Equation **A10** for each iteration of the resample (Winter 2017a). The CV of M from the 10000 random resamples was:

$$CV_M \qquad = \qquad SD_M / Mean_M$$

$$CV_M \qquad = \qquad 0.0021 / 0.0134 \quad = \quad 15.46\% \qquad\qquad \textbf{(A11)}$$

CV_M over the aggregate number of unassessed days between survey end and commercial season start was then added to the CV of the biomass prior estimate and the CV of variability in vessel catches on start day (Equations **A5-N** and **A5-S**). CV_M was further expressed as an absolute value and indexed by sign(1 - CV_M) to ensure that the value could not decrease if CV_M was hypothetically > 100%.

Time series model comparisons

Figure A3-S [next page]. South *D. gahi* biomass time series estimated from Bayesian posterior of the depletion model ± 95% confidence intervals. Solid lines, 45° striations: model parametrization with separate catchabilities q_{NSED} and q_{SED} (equivalent to Figure 8). Broken lines, 135° striations: model parametrization with single catchability q. Orange under-shading: mandatory use of SEDs (equivalent to Figure 4).

Figure A3-N [next page]. North *D. gahi* biomass time series estimated from Bayesian posterior of the depletion model ± 95% confidence intervals. Solid lines and 45° striations: model parametrization with separate catchabilities q_{NSED} and q_{SED} (equivalent to Figure 10). Broken lines and 135° striations: model parametrization with single catchability q. Orange under-shading: mandatory use of SEDs (equivalent to Figure 4). Yellow under-shading: early closure of the north sub-area (equivalent to Figure 4).

South
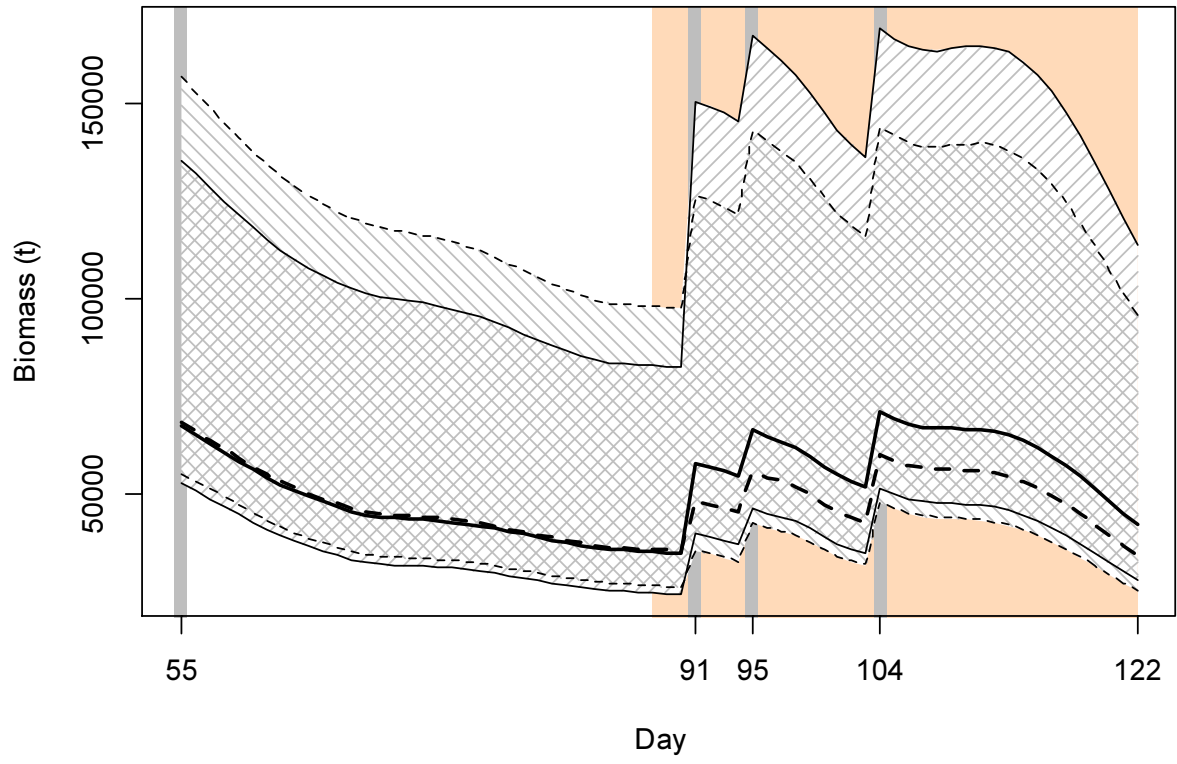
North
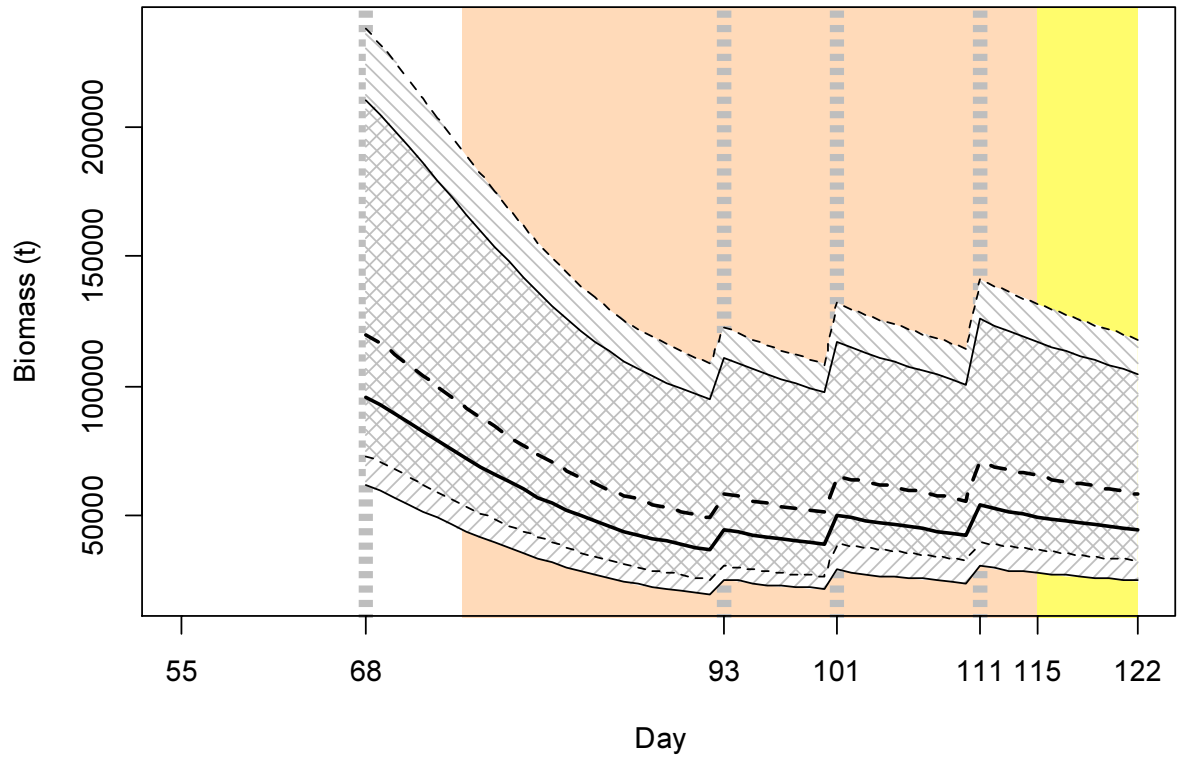
Total catch by species

Table A1: Total reported catches and discard by taxon during first season 2019 C-license fishing, and number of catch reports in which each taxon occurred. Does not include incidental catches of pinnipeds or seabirds.

Species Code	Species / Taxon	Catch Wt. (KG)	Discard Wt. (KG)	N Reports
LOL	*Doryteuthis gahi*	55585600	19123	953
PAR	*Patagonotothen ramsayi*	257246	256812	880
HAK	*Merluccius hubbsi*	124369	7872	433
BAC	*Salilota australis*	17714	1232	171
RAY	Rajiformes	7310	6919	401
CGO	*Cottoperca gobio*	7123	7123	393
BLU	*Micromesistius australis*	6855	6855	5
ILL	*Illex argentinus*	5322	2263	267
TOO	*Dissostichus eleginoides*	4841	2508	214
KIN	*Genypterus blacodes*	3031	1565	203
GRV	*Macrourus* spp.	2840	2560	39
PTE	*Patagonotothen tessellata*	2836	3197	46
MUN	*Munida* spp.	1875	1875	63
WHI	*Macruronus magellanicus*	1561	1561	44
MED	Medusae sp.	1092	1092	70
DGH	*Schroederichthys bivius*	1086	1079	150
ALF	*Allothunnus fallai*	692	692	64
PYM	*Physiculus marginatus*	620	620	3
POR	*Lamna nasus*	533	483	9
PAT	*Merluccius australis*	518	51	14
SCA	Scallop	273	273	15
ING	*Moroteuthis ingens*	235	235	53
UCH	Sea urchin	166	166	14
BUT	*Stromateus brasiliensis*	153	153	23
SPN	Porifera	80	80	13
CHE	*Champsocephalus esox*	79	79	23
GRF	*Coelorhynchus fasciatus*	62	62	8
DGS	*Squalus acanthias*	45	45	7
GRC	*Macrourus carinatus*	45	45	8
OCT	*Octopus* spp.	44	44	10
SAR	*Sprattus fuegensis*	37	37	12
SEP	*Seriolella porosa*	24	24	13
LAR	*Lampris immaculatus*	14	14	1
MUL	*Eleginops maclovinus*	14	14	6
MYX	*Myxine* spp.	11	11	5
GRH	*Macrourus holotrachys*	9	9	3
RED	*Sebastes oculatus*	8	8	3
OTH	–	5	5	1
DGX	Dogfish / Catshark	4	4	1
EEL	*Iluocoetes fimbriatus*	3	3	1
BDU	*Brama dussumieri*	1	1	1
Total		56034376	326794	953

Trawl area coverage

Area coverage was defined as the length of trawls × their trawl door width. For each of the 2685 trawls taken during the season (Figure 3), trawl door widths were obtained from the vessels' fishing reports. Missing trawl door widths were assigned as the average for that vessel for the season. The area cover of each trawl was then calculated as the rectangle of half the trawl width on either side of the start to end positions recorded for the trawl. This calculation implies the trawl to have been linear. However, if the Euclidean (straight-line) distance between start and end position was less than 80% of the trawl's timed distance (duration × average speed), the trawl was assumed to have turned, and for calculation was split on a pivot point. As turns are not reported, there is no direct way to infer the pivot point. Instead, the pivot point was optimized as the coordinate that produced an aggregate distance to the trawl start position + to the trawl end position most closely matching the timed distance of the trawl, with the constraint that this coordinate could not lie outside the 'box' of where the vessel had been over the period from the day before to the day after.

The rectangular areas of all trawls and split-trawls were then projected onto the Loligo Box. To estimate the areal proportion covered, the Loligo Box was discretized on a scale of 3 × 3 m. To make the amount of data points this produced tractable, the Loligo Box was further subdivided into grids of 5 × 5 km. As border grids intersected the Loligo Box, for each grid the actual number of points located within the Loligo Box (maximum (5000 × 5000)/(3 × 3) = 2778889 points) was first calculated by using the 'point.in.polygon' function of R package 'sp' (Pebesma et al. 2018), both on the delineation of the Loligo Box (inclusively) and on the delineation of the Beauchêne Island Zone (exclusively). Then, any points were eliminated that corresponded to water depth of <10 m, interpolated from a GEBCO_08 30 arc-second bathymetry grid (British Oceanographic Data Centre). Finally, the grid was looped through the projection of each trawl and split-trawl area by turn[1], and again using 'point.in.polygon', the points covered by each trawl / split-trawl were iteratively summed. For all rectangulations and area calculations, coordinates were converted to WGS 84 projection in UTM sector 21F using R library 'rgdal' (proj.maptools.org).

Outputs derived from the calculations were the total area proportion of the Loligo Box trawled, the cumulative numbers of trawl passes over any proportion of the Loligo Box, the concentration of *D. gahi* catch by area proportion of the Loligo Box, and the concentration of effort by area proportion of the Loligo Box.

---

[1] In practice, to reduce computer time subsets of trawls were preselected that intersected each given grid.